Wang *et al. Microstructures* **2025**, *5*, 2025074
**DOI:** 10.20517/microstructures.2024.116

**Microstructures**

**Review**

**Open Access**

Check for updates

# Recent advances in non-metal doped ZnS nanostructures for photocatalytic hydrogen production

**Shuo Wang[1,2], Xiaowei Niu[1], Lin Wang[2], Jinghui Bi[3], Weiyou Yang[2], Huilin Hou[2]**

[1]Key laboratory of Ecological Restoration of Regional Contaminated Environment, Ministy of Education, College of Environment, Shengyang University, Shenyang 110044, Liaoning, China.
[2]Institute of Micro/Nano Materials and Devices, Ningbo University of Technology, Ningbo 315211, Zhejiang, China
[3]School of Applied Science, Taiyuan University of Science and Technology, Taiyuan 030024, Shanxi, China.

**Correspondence to:** Dr. Xiaowei Niu, 21 Wanghua South Street, Dadong District, Shenyang, Liaoning Province, China. E-mail: niuxiaowei@syu.edu.cn; Prof. Huilin Hou, Institute of Micro/Nano Materials and Devices, Ningbo University of Technology, 201 Fenghua Road, Jiangbei District, Ningbo 315211, Zhejiang, China. E-mail: houhuilin@nbut.edu.cn; Dr. Jinghui Bi, School of Applied Science, Taiyuan University of Science and Technology, Waliu Road 66, Wanbailin District, Taiyuan 030024, Shanxi, China. E-mail: 2001001@tyust.edu.cn

**How to cite this article:** Wang, S.; Niu, X.; Wang, L.; Bi, J.; Yang, W.; Hou, H. Recent advances in non-metal doped ZnS nanostructures for photocatalytic hydrogen production. *Microstructures* **2025**, *5*, 2025074. https://dx.doi.org/10.20517/microstructures.2024.116

**Received:** 11 Nov 2024 **First Decision:** 2 Dec 2024 **Revised:** 17 Dec 2024 **Accepted:** 25 Dec 2024 **Published:** 17 Jun 2025

**Academic Editor:** Chunqiang Zhuang **Copy Editor:** Shu-Yuan Duan **Production Editor:** Shu-Yuan Duan

## Abstract

Photocatalytic hydrogen production is a sustainable approach to addressing energy and environmental issues, with ZnS being a prominent photocatalyst due to its efficiency, stability, and affordability. However, its wide bandgap and quick carrier recombination hinder its performance. Non-metal doping, particularly with nitrogen and carbon, has been shown to enhance electronic structure, light absorption, and charge separation of ZnS, thus improving its photocatalytic activity. This review highlights the advancements in nitrogen-doped, carbon-doped, and carbon-nitrogen co-doped ZnS, emphasizing nitrogen's significant impact on bandgap reduction and charge transfer, and carbon's role in promoting heterojunctions and active sites. Co-doping further amplifies these effects, leading to superior photocatalytic performance. The review also discusses performance variations among catalysts, the effects of synthesis methods and reaction conditions, and the role of auxiliary agents. Future research should concentrate on comparing doping methods, optimizing synthesis, and exploring phase-dependent activities to maximize the potential of ZnS-based photocatalysts. This work highlights the benefits of non-metal doped ZnS in hydrogen production and outlines key challenges and future research directions in the field.

**Keywords:** ZnS, photocatalytic hydrogen production, doping, non-metal

## INTRODUCTION

The escalating global population and industrialization have heightened the demand for energy, predominantly from fossil fuels such as coal, oil, and natural gas[1,2], which, despite driving economic growth and improving living standards, are finite and cause environmental damage[3,4]. Their overuse jeopardizes energy security and sustainability[5,6], and their combustion contributes to air pollution and greenhouse gas emissions, notably $CO_2$, which worsens climate change[7,8]. To mitigate these issues, there is a growing focus on renewable energy sources such as solar, wind, and hydropower that minimize environmental impact[9,10]. Photocatalytic reactions are crucial for environmental protection and energy production[11,12]. They can degrade water pollutants into harmless substances[13,14] and are used in wastewater treatment processes, improving water quality[15,16]. Photocatalytic technology also reduces $CO_2$ to hydrocarbons and is being explored for solar hydrogen production and solar cells[17]. Photocatalytic hydrogen production, which uses light to split water into hydrogen, is a promising solution for energy sustainability and environmental protection[18]. When photons exceed the semiconductor's bandgap, they are absorbed, causing electrons to move from the valence band (VB) to the conduction band (CB), creating holes. The built-in electric field in semiconductor photocatalysts separates charges, with photogenerated electrons combining with protons on the surface to form hydrogen[19].

Zinc sulfide (ZnS), a II-VI semiconductor, has garnered significant attention as a promising photocatalyst due to its favorable optoelectronic properties[20]. ZnS possesses a wide bandgap of approximately 3.6 eV, allowing it to absorb ultraviolet (UV) light and generate electron-hole pairs. These electron-hole pairs are critical for driving the redox reactions necessary for water splitting and hydrogen generation. The process of light-driven water splitting on ZnS begins when the photon energy exceeds the bandgap energy of the semiconductor. Upon UV light absorption, electrons in the VB are excited to the CB, creating electron-hole pairs. The photogenerated electrons in the CB participate in the reduction reaction by combining with protons ($H^+$) adsorbed on the ZnS surface to produce hydrogen gas ($H_2$). Simultaneously, the holes left in the VB drive the oxidation of water ($H_2O$) to generate oxygen gas ($O_2$). However, the efficiency of this process depends heavily on minimizing the recombination of these photogenerated electrons and holes, which otherwise reduces the photocatalytic performance. To raise the performance of ZnS photocatalysts, several key factors must be addressed. First, enhancing light absorption by narrowing the bandgap is critical, as the current wide bandgap of ZnS limits absorption to the UV region, which represents only a small fraction of the solar spectrum. Non-metal doping, for instance, modifies the electronic structure of ZnS, enabling visible-light absorption and expanding the range of usable solar energy. Second, improving charge separation and transfer is essential to prevent electron-hole recombination. Strategies such as introducing surface defects, doping, or constructing heterojunctions help create surface states that trap charges and facilitate their migration to reaction sites[21]. Lastly, improving the stability of ZnS is crucial to mitigating photocorrosion, which often degrades the material's performance during prolonged photocatalysis. Non-metal doping stands out as an effective method for improving ZnS photocatalysts. By introducing non-metal elements such as nitrogen (N), sulfur (S), carbon (C), or fluorine (F) into the ZnS lattice[22-27], these dopants modify the electronic structure of ZnS, narrowing its bandgap and extending its light absorption into the visible spectrum[28]. This modification allows ZnS to harness a broader portion of the solar spectrum, thereby increasing its photocatalytic efficiency. Furthermore, non-metal doping enhances charge separation and improves the overall stability of ZnS during photocatalysis, addressing issues such as photocorrosion, which can lead to performance degradation over time[24].

Significant advancements have been achieved in the synthesis and application of non-metal doped ZnS nanostructures for photocatalytic hydrogen production. Research has demonstrated that doping ZnS with non-metal elements can precisely tune its optoelectronic properties, resulting in improved visible light

absorption, enhanced charge separation, and overall higher photocatalytic efficiency[21,22,29,30]. To achieve these improvements, various synthesis techniques - such as hydrothermal processes, sol-gel methods, and chemical vapor deposition (CVD) - have been employed to control both the concentration and uniform distribution of dopants within the ZnS lattice, thereby optimizing its photocatalytic performance[31,32]. This review provides a comprehensive summary of recent progress in the synthesis and application of non-metal doped ZnS nanostructures for photocatalytic hydrogen production [Figure 1]. It highlights the unique advantages of non-metal doping, such as bandgap narrowing and improved charge carrier dynamics, which enable ZnS to extend its light absorption into the visible spectrum while enhancing photocatalytic stability. Moreover, the review identifies the key challenges that remain, including the need to improve doping efficiency, long-term stability, and photocorrosion resistance for practical applications. While ZnS-based photocatalysts have been extensively studied for photocatalytic water splitting and related applications, the majority of previous research has focused on heterojunction construction, surface loading, or metal element doping as modification strategies. In contrast, studies specifically investigating non-metal doping for ZnS-based photocatalytic hydrogen production remain extremely limited. Despite the abundance of reviews on ZnS photocatalysts, there is a notable lack of reviews dedicated to exploring non-metal doping in this context. This article addresses this gap by providing a focused and detailed review of non-metal doped ZnS photocatalysts. It systematically analyzes the advancements, advantages, and mechanisms of non-metal doping compared to conventional modification methods. By bridging the deficiencies in current literature, this review identifies opportunities for future research aimed at enhancing the efficiency, stability, and practical applicability of ZnS photocatalysts for hydrogen production. Finally, it offers insights into potential development trends, emphasizing the critical role of non-metal doping in advancing sustainable energy conversion technologies.

## THE ROLE AND IMPACT OF NON-METAL DOPING ON BANDGAP MODULATION IN ZNS NANOSTRUCTURES FOR PHOTOCATALYTIC HYDROGEN PRODUCTION

### Introduction to non-metal doping: advantages over metal doping

In recent years, photocatalytic hydrogen production using ZnS nanostructures has garnered significant attention due to its potential in sustainable energy generation[33]. However, pristine ZnS suffers from limitations, including a wide bandgap (~ 3.6 eV), which restricts its absorption to the UV region, accounting for only a small fraction of the solar spectrum[23]. To address this limitation, doping strategies, including metal and non-metal doping, have been employed to enhance the photocatalytic performance of ZnS by modulating its electronic structure, improving charge separation, and extending its absorption range into the visible light region[28].

Non-metal doping has distinct advantages over metal doping in photocatalytic systems, particularly for ZnS nanostructures:

(1) Reduced recombination rate: Non-metal dopants typically introduce localized energy states near the conduction or VBs, which can trap photogenerated electrons and holes, thereby reducing their recombination rate. In contrast, metal doping often creates deeper trap states that may facilitate charge recombination, leading to a decrease in overall efficiency[34].

(2) Minimized defects and enhanced stability: Metal dopants can induce lattice distortions, resulting in the formation of defects that act as recombination centers and compromise the material's stability[35,36]. Non-metal doping, especially with elements such as nitrogen, carbon, or sulfur, typically results in a more stable lattice structure with fewer undesirable defects[22,29,30].

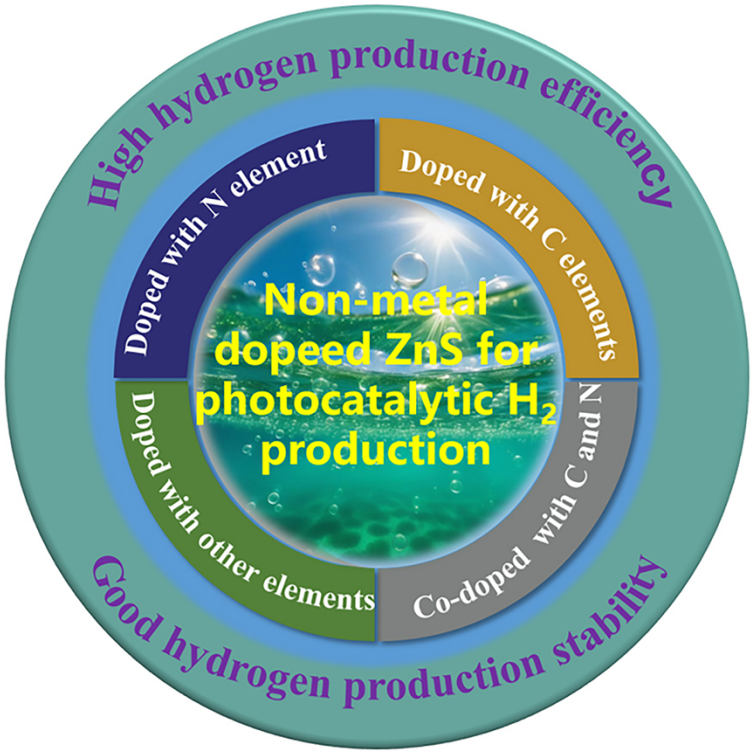


**Figure 1.** Main content of this review work.

(3) Cost-effectiveness and environmental friendliness: Non-metals, such as nitrogen, sulfur, and phosphorus (P), are abundant, cost-effective, and less toxic compared to many transition metals commonly used for doping. This makes non-metal doping a more sustainable and environmentally friendly option, especially for large-scale hydrogen production applications[37].

### Essential impact of non-metal doping on photocatalysis

The essential impact of non-metal doping on photocatalysis, particularly in ZnS nanostructures, lies in its ability to modify the material's electronic structure. This modification enhances light absorption, promotes charge separation, and improves overall photocatalytic efficiency. Non-metal doping primarily affects the bandgap of ZnS, which is a key factor in determining its photocatalytic performance[38]. The mechanisms by which non-metal doping affects photocatalysis can be summarized as follows:

(1) One of the most significant effects of non-metal doping is the reduction of the bandgap in ZnS. Non-metals introduce additional electronic states, such as mid-gap states, within the forbidden energy gap of ZnS. These states lower the energy required for electrons to transition from the VB to the CB, thereby narrowing the bandgap and extending ZnS's absorption range into the visible region[39,40]. For instance, nitrogen doping in ZnS introduces localized states near the VB, which lowers the overall bandgap by promoting transitions from these states. This results in improved absorption in the visible light spectrum, significantly enhancing photocatalytic hydrogen production under solar irradiation[26,27,30].

(2) Non-metal dopants can act as traps for electrons or holes, facilitating the separation of photogenerated charge carriers and suppressing their recombination. Efficient charge separation is crucial for improving photocatalytic efficiency, as it allows more electrons and holes to actively participate in the hydrogen

production process[41,42]. For example, sulfur doping in ZnS has been reported to introduce shallow trap states that facilitate charge separation, leading to improved photocatalytic activity.

(3) Non-metal doping can alter the surface chemistry of ZnS nanostructures, creating new active sites that enhance the adsorption of reactant molecules, such as water and $CO_2$[43]. Doping with elements such as carbon or phosphorus can create surface defects or unsaturated bonds, which enhance the interaction between the catalyst surface and the reactants, improving the overall photocatalytic hydrogen production efficiency[24,29,30,44].

## BANDGAP MODULATION THROUGH NON-METAL DOPING

The primary focus of non-metal doping in ZnS nanostructures is to modulate the bandgap and shift the absorption edge from the UV to the visible light region [Figure 2][45]. This section will discuss various non-metal doping methods and their effects on bandgap tuning, highlighting the most effective strategies for enhancing photocatalytic performance.

### Nitrogen doping

Nitrogen is a widely used non-metal dopant for ZnS, enhancing photocatalytic hydrogen production under visible light by reducing the bandgap and improving charge separation efficiency. Peng *et al.*[30] synthesized N-doped carbon-coated ZnS (ZnS@N-C) with sulfur vacancies ($V_S$) for visible-light-driven photodegradation of tetracycline hydrochloride (TCH). Nitrogen doping alters the electronic structure of the carbon material due to differences in electronegativity between nitrogen and carbon, redistributing the electron cloud and enhancing charge transfer at the carbon-ZnS interface. The lone pair electrons on nitrogen atoms participate in the conjugated system, increasing electron delocalization and modifying the electronic density of states. This introduces intermediate states within the ZnS bandgap, facilitating electron transitions and improving photocatalytic performance [Figure 3A]. $V_S$ further influences the band structure by lowering the CB position, reducing the bandgap from 3.32 eV to 3.06 eV, as confirmed by X-ray photoelectron spectroscopy (XPS) [Figure 3B-F]. Riazian *et al.*[46] demonstrated that nitrogen doping introduces new electronic states near the VB, raising its energy while minimally impacting the CB, leading to bandgap reduction [Figure 4A]. Additionally, nitrogen doping induces lattice defects, distorting the crystal structure, which broadens X-ray diffraction (XRD) peaks and modifies the periodic potential field, further altering the band structure and contributing to the bandgap narrowing [Figure 4B and C].

### Carbon doping

Carbon doping is an effective strategy for modulating the bandgap of ZnS. Carbon can replace sulfur or zinc atoms in the ZnS lattice, creating shallow donor states near the CB, which narrows the bandgap and enhances visible light absorption. Additionally, carbon-doped ZnS nanostructures exhibit improved stability and photocatalytic activity due to bandgap narrowing and increased surface reactivity[47]. Zhang *et al.*[22] synthesized ZnS-CdSe@Co/N-C core/shell composites for $CO_2$ photoconversion under visible light. ZnS, with a bandgap of 3.6 eV, absorbs only UV light, while CdSe, with a tunable bandgap (1.8-3.0 eV), absorbs visible light. Combining ZnS with CdSe forms a heterogeneous structure, optimizing the overall bandgap. UV-visible (Vis) diffuse reflectance spectra and Tauc plots showed that N-doped carbon spheres have a bandgap of 2.33 eV, which further decreases to 2.03 eV in the ZnS-CdSe@Co/N-C composite, significantly improving visible light absorption [Figure 5A and B]. The N-doped carbon spheres possess a p-p conjugated structure that promotes electron-hole separation when ZnS-CdSe nanoparticles are dispersed on their surface. Their inherent conductivity and heteroatom doping facilitate efficient electron extraction and bandgap tuning, enhancing photocatalytic performance [Figure 5C].

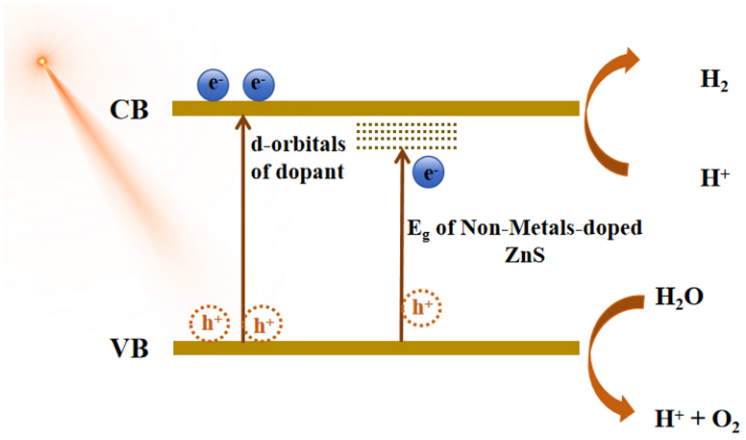


**Figure 2.** Schematic diagram of photocatalysis after adjustment of the band gap by non-metallic doped ZnS. CB: Conduction band; VB: valence band; ZnS: Zinc sulfide.

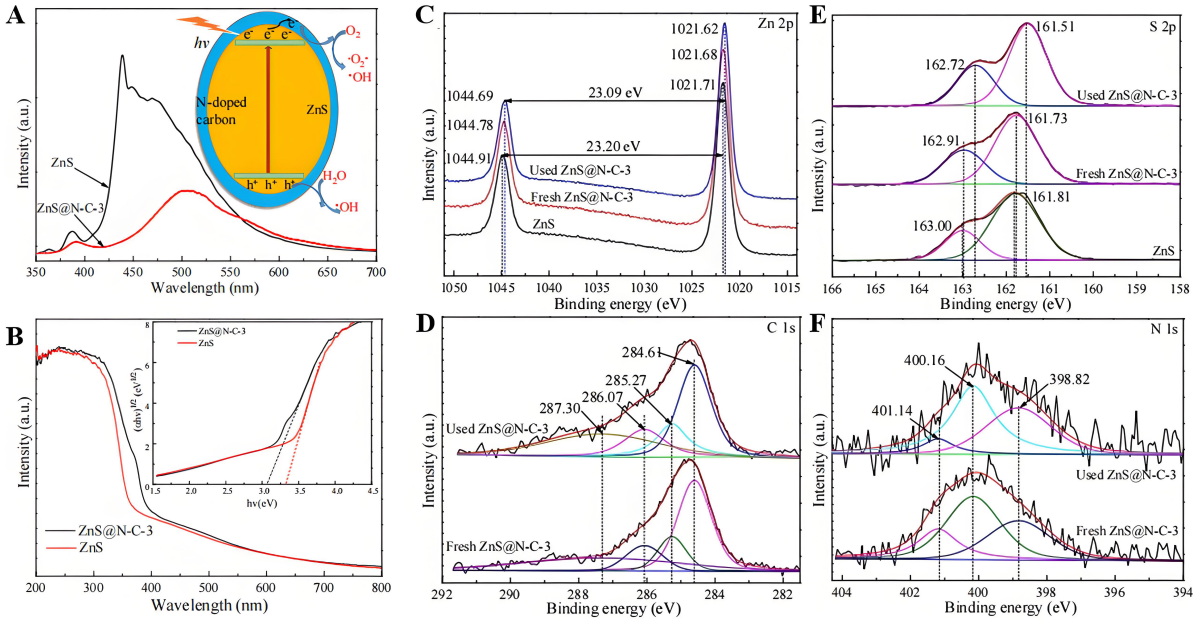


**Figure 3.** (A) PL spectrum and photocatalytic mechanism of ZnS@N-C-3; (B) UV-Vis DRS spectra and band gap analysis plot of ZnS and ZnS@N-C-3; Zn 2p (C); S 2p (E); C 1s (D); and N 1s (F) XPS spectra of ZnS and fresh and used ZnS@N-C-3. Copyright 2019, MDPI[30]. PL: Photoluminescence; ZnS: Zinc sulfide; UV-Vis: ultravoilet-visble; DRS: diffuse reflectance spectroscopy; XPS: X-ray photoelectron spectroscopy.

## Phosphorus doping

Phosphorus-doped ZnS exhibits superior photocatalytic performance due to enhanced visible light absorption, improved charge separation, and greater chemical stability, making it ideal for long-term hydrogen production. Zhu *et al.*[48] synthesized a P-doped g-$C_3N_4$/ZnS (PCN/ZnS) composite via a solvothermal method to investigate its photocatalytic degradation of tetracycline (TC) under visible light. Phosphorus atoms, likely substituting specific atomic sites within the ZnS lattice, alter the local electronic environment and interatomic interactions, thereby influencing the bandgap. XRD analysis showed shifts in peak positions and intensities, indicating disturbances in crystal periodicity and symmetry [Figure 6A-C].

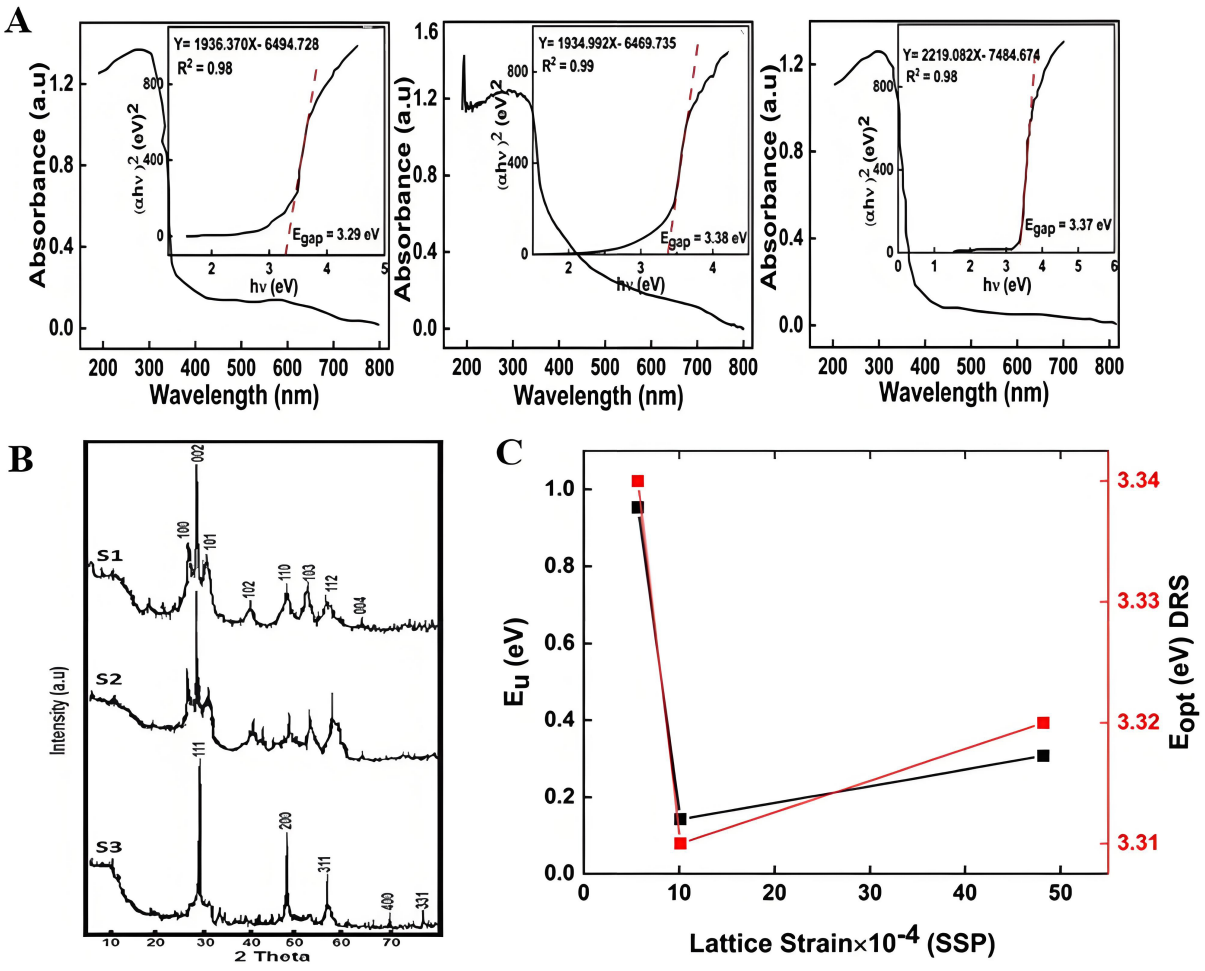


**Figure 4.** (A) The DRS spectra of ZnS NPs and the inset indicate the Eopt of the Tauc's evaluation from the curve of $(\alpha h\nu)^2$ *vs.* (hν) for S1, S2 and S3; (B) XRD patterns of the wurtzite and zinc blend crystallite phases of the ZnS synthesized NPs; (C) Variation of the lattice strain with the optical band gap which is determined from DRS and the Urbach energy. Copyright 2023, IOPScience[46]. DRS: Diffuse reflectance spectroscopy; ZnS: Zinc sulfide; NP: nanoparticles; XRD: X-ray diffraction.

These structural changes redistribute electron bands, affecting electron confinement and scattering within the crystal. Additionally, phosphorus doping introduces new electronic states that interact with existing states, modifying the valence and CB edges. XPS revealed shifts in binding energy, reflecting changes in electron density and electronic states [Figure 6D-H]. This hybridization of new and original states alters the energy required for electron transitions, effectively reducing the bandgap [Figure 6I and J].

### Fluorine doping

Fluorine doping enhances ZnS properties by substituting sulfur atoms in the lattice, introducing shallow acceptor levels that facilitate electron transitions under visible light, thereby improving photocatalytic hydrogen production and $CO_2$-to-CO conversion performance[49,50]. Bao *et al.*[50] synthesized fluorine-doped ZnS catalysts with $V_S$ via a hydrothermal method. Fluorine doping primarily modulates the ZnS bandgap through lattice distortion, atomic size effects, and electronic structure changes. Due to fluorine's smaller atomic radius, lattice constants and atomic interactions are altered, shifting VB and CB positions. Additionally, fluorine's high electronegativity redistributes the electron cloud, introducing new electronic states near the VB or CBs. These impurity states provide alternative pathways for electron transitions, effectively reducing the functional bandgap [Figure 7A and B]. The synergistic effect of fluorine doping and

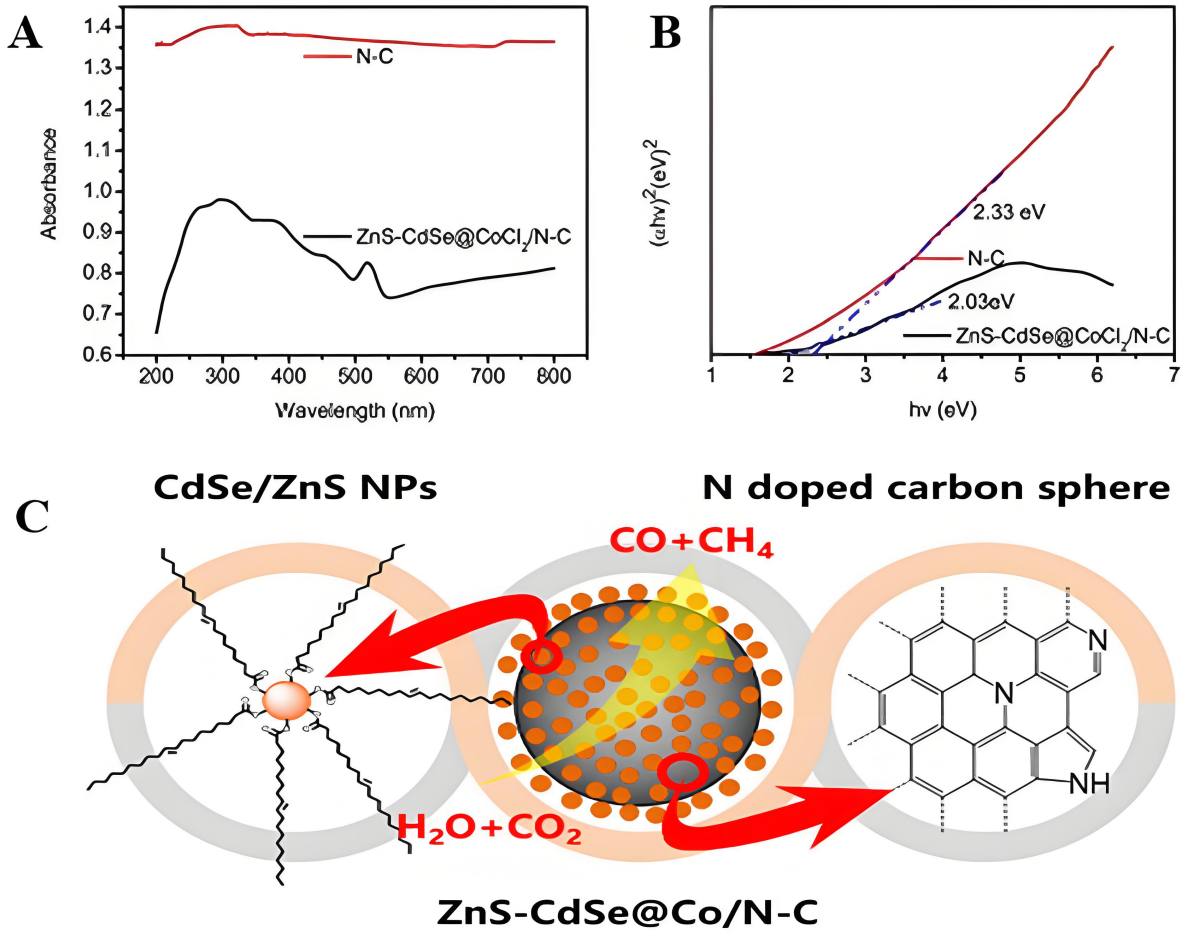


**Figure 5.** (A) The UV-Vis spectra of ZnS-CdSe@Co/N-C; (B) the transformed Tauc plot of ZnS-CdSe@Co/N-C; (C) Preparation and working mechanism of ZnS-CdSe@Co/N-C core/shell composites. Copyright 2023, Royal Society of Chemistry[22]. UV-Vis: Ultraviolet-visible; ZnS: Zinc sulfide.

$V_S$ enhances photogenerated carrier separation, further improving photocatalytic performance [Figure 7C and D]. Experimental results show an extended light absorption range (400-800 nm) and bandgap variation with fluorine content. Theoretical calculations of adsorption energy, charge density, and electronic structure provide deeper insight into the mechanisms of fluorine doping. Further studies are needed to quantify the precise degree of bandgap adjustment.

### The relationship between bandgap adjustment and photocatalytic hydrogen production

The adjustment of the bandgap of ZnS through doping with non-metallic elements exerts a significant impact on its photocatalytic hydrogen production performance[51]. These effects primarily include alterations in the light absorption range, optimization of photogenerated carrier behavior, and modifications of surface properties. Each of these factors is interconnected and collectively influences the overall photocatalytic hydrogen production process. By expanding the absorption spectrum, doping enables ZnS to utilize a broader range of the solar spectrum, thus enhancing light absorption efficiency. Moreover, doping can improve the separation and migration of photogenerated charge carriers, reducing recombination losses and increasing the availability of electrons for the hydrogen evolution reaction. Additionally, non-metallic doping can modify the surface characteristics of ZnS, such as increasing active sites or improving charge transfer efficiency, which further contributes to enhanced photocatalytic activity.

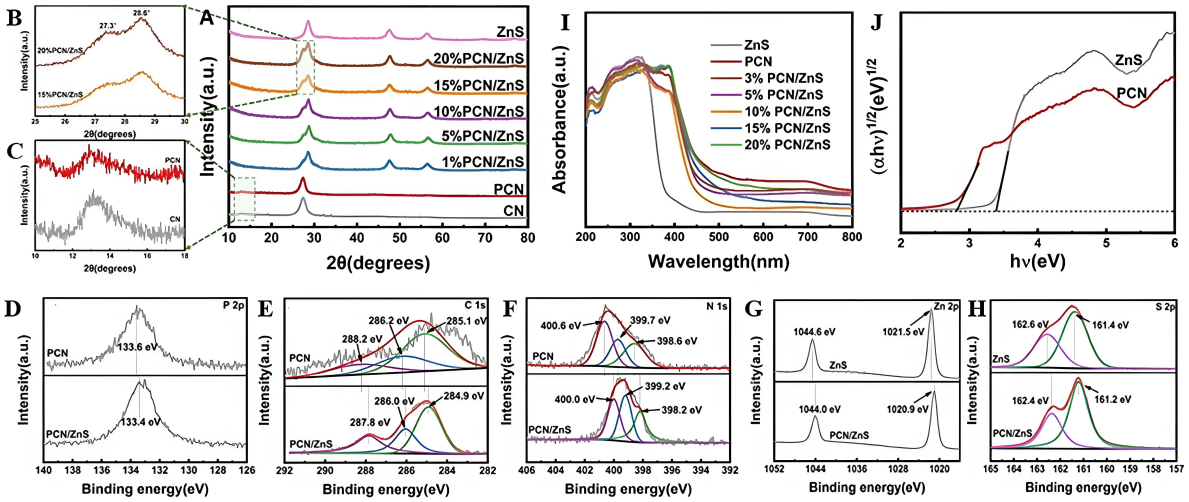


**Figure 6.** (A) XRD patterns of PCN, ZnS and x%PCN/ZnS. (B and C) Partially enlarged XRD patterns; XPS spectra of (D) P 2p; (E) C 1s; (F) N 1s; (G) Zn 2p; (H) S 2p for PCN, ZnS and PCN/ZnS; (I) UV-Vis diffuse reflectance spectra of PCN, ZnS and x%PCN/ZnS. (J) The band gaps (Eg) of PCN and ZnS. Copyright 2022, Elsevier[48]. XRD: X-ray diffraction; PCN: P-doped g-$C_3N_4$; ZnS: Zinc sulfide; UV: ultraviolet.

These synergistic effects provide multiple avenues to improve the efficiency of photocatalytic hydrogen production, making doped ZnS a promising material for sustainable energy applications.

## SYNTHESIS AND CHARACTERIZATION METHODS

### Synthesis methods of non-metal doped ZnS nanostructures

Non-metal doped ZnS nanostructures can be synthesized through various techniques, including hydrothermal, solvothermal, sol-gel, microwave-assisted, and ultrasonic-assisted methods. Hydrothermal and solvothermal methods involve reactions in aqueous or organic solvents under high temperature and pressure, allowing precise control over morphology and achieving high-purity, monodispersed nanostructures, such as spheres, nanosheets, and nanotubes[48,52-60]. The sol-gel method, which involves hydrolysis and polycondensation, offers excellent control over nanomaterial properties, typically producing nearly spherical ZnS with tunable morphology based on reaction parameters such as pH and precursor concentration[61-73]. Microwave-assisted synthesis uses high-frequency electromagnetic radiation to uniformly heat the reaction mixture, reducing synthesis time and providing uniform ZnS spheres with controlled dopant distribution[36]. Ultrasonic-assisted synthesis utilizes high-intensity ultrasound waves, generating localized hot spots that accelerate chemical reactions and improve dopant dispersion within the ZnS lattice, resulting in nanostructures with controlled size and morphology[74-76].

### Characterization techniques

To evaluate the structural and photocatalytic properties of non-metal doped ZnS nanostructures, several characterization techniques are employed. XRD is used to analyze the crystal structure and confirm phase purity. XPS provides detailed information on the chemical composition and confirms the incorporation of dopants into the ZnS lattice. UV-Vis diffuse reflectance spectroscopy (DRS) measures the optical properties and helps determine the bandgap, providing insights into the light absorption capabilities. Photoluminescence (PL) spectroscopy studies the recombination dynamics of photogenerated charge carriers, while electrochemical impedance spectroscopy (EIS) assesses charge carrier mobility and the efficiency of electron-hole pair separation, which directly correlates with photocatalytic performance.

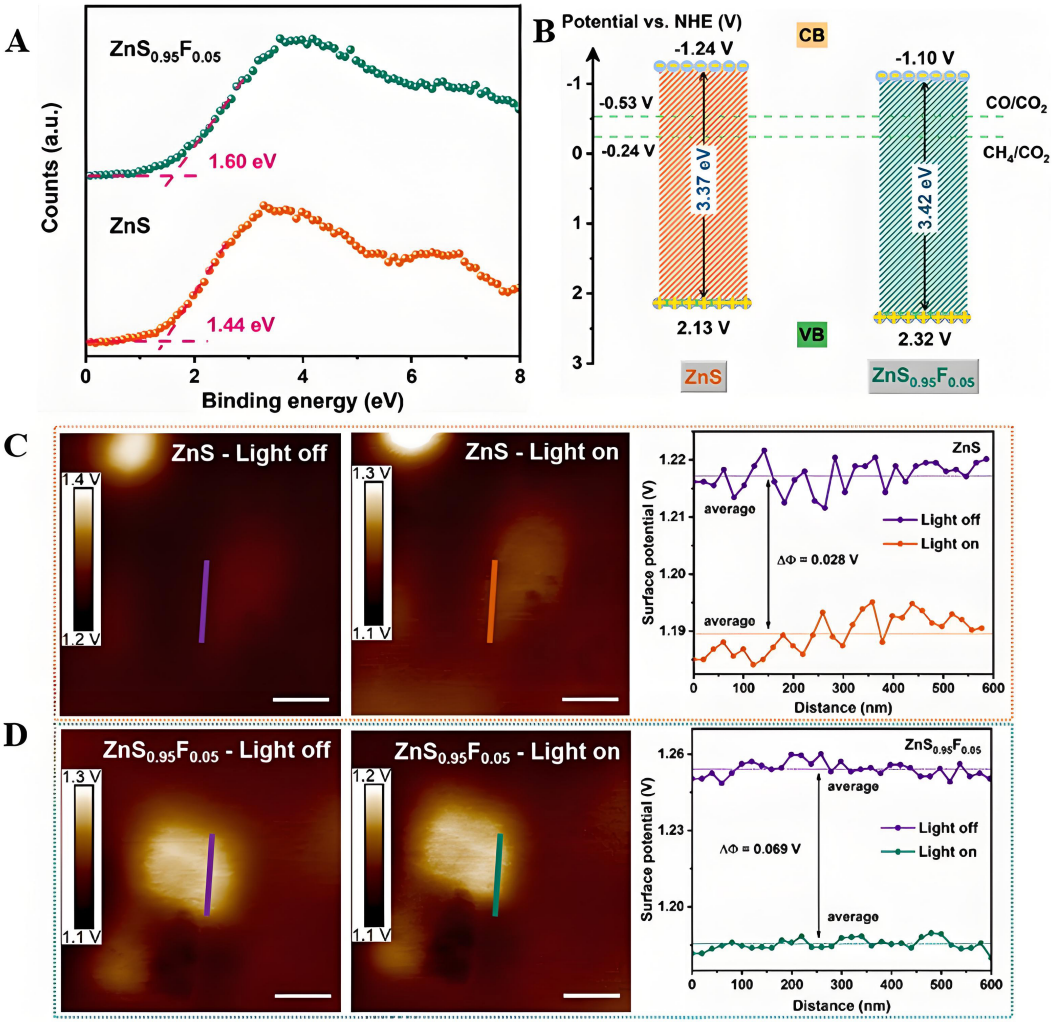


**Figure 7.** (A) VBXPS; and (B) band alignment for ZnS and $ZnS_{0.95}F_{0.05}$. KPFM potential images in the dark and under illumination, plot of the surface potential measured in the dark and under illumination for (C) ZnS and (D). Copyright 2024, Elsevier[50]. VBXPS: Valence band X-ray photoeletron spectroscopy; ZnS: Zinc sulfide; KPFM: Kelvin probe force microscopy.

## NON-METAL DOPED ZNS NANOSTRUCTURES USED IN PHOTOCATALYTIC HYDROGEN PRODUCTION

In recent years, non-metal doped ZnS nanostructures have made notable progress in the field of photocatalytic hydrogen production. These doped nanostructures exhibit enhanced catalytic efficiency due to their modified electronic structures and improved charge separation capabilities. Table 1 summarizes the performance of various reported non-metal doped ZnS materials. In this chapter, we will provide a detailed discussion of different doping strategies, including nitrogen, carbon, co-doping with carbon and nitrogen, and other elements, to explore their impact on photocatalytic hydrogen production.

### Nitrogen-doped ZnS

N-doped ZnS is a promising photocatalyst for solar energy conversion, particularly in hydrogen production. Its enhanced photocatalytic activity comes from an optimized electronic structure that broadens light absorption into the visible spectrum and promotes efficient charge carrier dynamics. Nitrogen doping introduces impurity states within the bandgap of ZnS, lowering the energy needed to excite electrons and

**Table 1. A summary of the reported performance of non-metal doped ZnS nanostructures for photocatalytic hydrogen production**

| Photocatalyst | Synthesis method | Sacrificial agent | Light source | $H_2$ production rate | Refs. |
|---|---|---|---|---|---|
| N-doped ZnS | Hydrothermal | 80 mL of aqueous lactic acid solution | 300 W Xe lamp | 243.61 $\mu molg^{-1} h^{-1}$ | [26] |
| NG-ZnS | Hydrothermal | 0.1 M $Na_2S$, 0.04 M $Na_2SO_3$ and 3 M NaCl | 300W Xe lamp (> 420nm) | 1,755.7 $\mu molg^{-1} h^{-1}$ | [23] |
| N-doped ZnS | Co-precipitation | methanol (10 vol. %) | 300 W Xe lamp | 25 $\mu molg^{-1} h^{-1}$ | [77] |
| N-doped ZnS/ZnO | Hydrothermal | 0.1 M $Na_2S$, 0.1 M $Na_2SO_3$ | 300 W Xe lamp (> 400nm) | 1,790 $\mu molg^{-1} h^{-1}$ | [24] |
| C-doped ZnS/ZnO/Rh | Hydrothermal | 50ml $Na_2S/Na_2SO_3$ | 200 W Xe lamp | 117 $\mu molg^{-1}h^{-1}$ | [44] |
| NCQDs/ZnS | Hydrothermal | 0.35 M $Na_2S$ 0.25 M $Na_2SO_3$ | No reported | 5,700 $\mu molg^{-1}h^{-1}$ | [27] |
| C, N-doped ZnS-thio | Hydrothermal | No sacrificial agents were used | 150 W Xe lamp | 176 $\mu molg^{-1}h^{-1}$ | [78] |
| C, N-doped ZnS | Hydrothermal | $Na_2S$ and $Na_2SO_3$ | 250 W Xe lamp | 999 $\mu molg^{-1} h^{-1}$ | [29] |
| C, N, O-doped ZnS | Hydrothermal | No sacrificial agents were used | No reported | 254.7 $\mu molg^{-1} h^{-1}$ | [79] |

ZnS: Zinc sulfide; NCQD: N-doped carbon quantum dot.

enabling absorption of visible light, which is a larger portion of the solar spectrum. This also improves the separation and transport of photogenerated charge carriers, reducing recombination losses and enhancing photocatalytic efficiency. The optimal nitrogen doping concentration significantly influences the photocatalytic performance of ZnS. A study by Tie *et al.*[26] found that 3% N-doped ZnS had the highest hydrogen production rate, attributed to a balance between light absorption and charge transfer efficiency [Figure 8A and B]. Higher nitrogen concentrations led to a decline in efficiency, possibly due to recombination centers or structural defects. N-doped ZnS also excels in degrading organic pollutants under sunlight, demonstrating its versatility for environmental remediation [Figure 8C-E]. The stability of the doped ZnS crystal structure is linked to its surface energy; nitrogen doping decreases surface energy, enhancing structural stability and improving the catalyst's resistance to corrosion and cycling stability [Figure 8F and G]. This stability is crucial for maintaining the catalyst's performance during photocatalytic processes.

Building on nitrogen doping, Azarang *et al.*[23] investigated the synergistic effects of combining N-doped ZnS with graphene, a highly conductive material known for its excellent electron mobility. They synthesized N-doped graphene-supported ZnS(NG-ZnS) nanorods using a two-step process: first preparing graphene oxide, then depositing ZnS and doping with nitrogen. This hybrid structure aimed to enhance photocatalytic performance by leveraging graphene's superior charge transport properties alongside the improved light absorption of N-doped ZnS. Characterization via XRD, high-resolution transmission electron microscopy (HRTEM), XPS, and Raman spectroscopy confirmed successful synthesis of NG-ZnS nanorods. Transmission electron microscopy (TEM) images revealed uniform nanorod morphology (120-150 nm) with no damage to the ZnS structure after nitrogen doping [Figure 9A and B]. Under visible light irradiation, NG-ZnS achieved a hydrogen production rate of 1,755.7 $\mu mol\ g^{-1}\ h^{-1}$, 14 times higher than pure ZnS and 2.3 times higher than graphene-supported ZnS (G-ZnS), demonstrating the significant impact of nitrogen doping and graphene support on photocatalytic efficiency [Figure 9C]. Additionally, NG-ZnS showed excellent stability, with minimal efficiency loss after four cycles of hydrogen production, highlighting its durability [Figure 9D]. However, N-doped ZnS photocatalysts face challenges with photocorrosion, particularly under UV light. The altered energy band structure from nitrogen doping increases the interaction between photogenerated holes and the catalyst surface, accelerating oxidative corrosion. As a result, the catalyst's performance deteriorates over time, typically after 12 h of testing. The proposed mechanism diagram of NG-ZnS for photocatalytic hydrogen production is shown in Figure 9E.

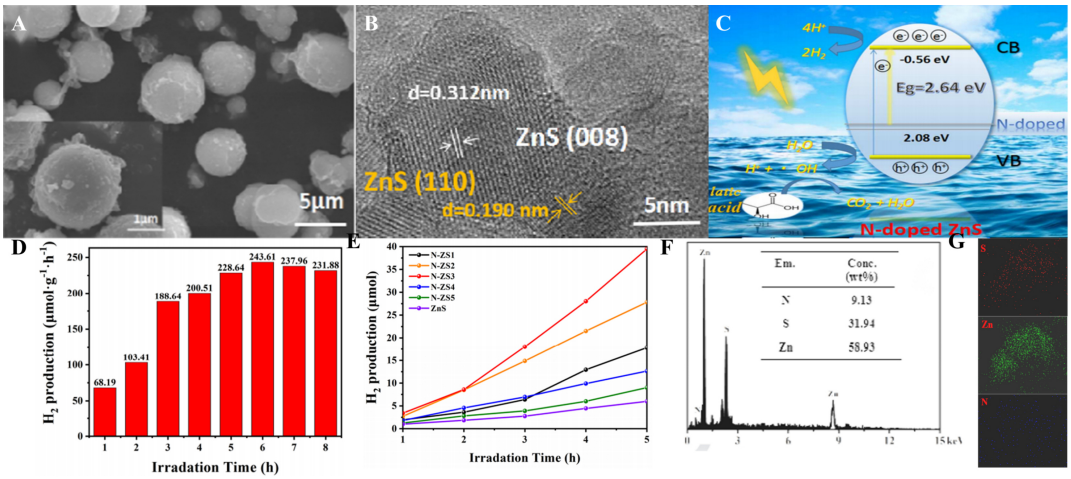


**Figure 8.** (A) The FE-SEM images of the N-ZS3 sample. (B) HRTEM observations of the N-ZS3 sample. (C)The photocatalytic $H_2$ production on the N-ZS3 sample. (D) The $H_2$ evolution rate for the N-ZS3 sample. (E) The time-dependent $H_2$ evolution of ZnS, N-ZS1, N-ZS2, N-ZS3, N-ZS4, and N-ZS5 samples. (F) The elemental composition of the N-ZS3 sample. (G) EDS mapping images. Copyright 2019, Elsevier[26]. FE-SEM: Field emission-scanning electron microscope; HRTEM: high-resolution transmission electron microscopy; EDS: energy dispersive X-ray specctroscopy.

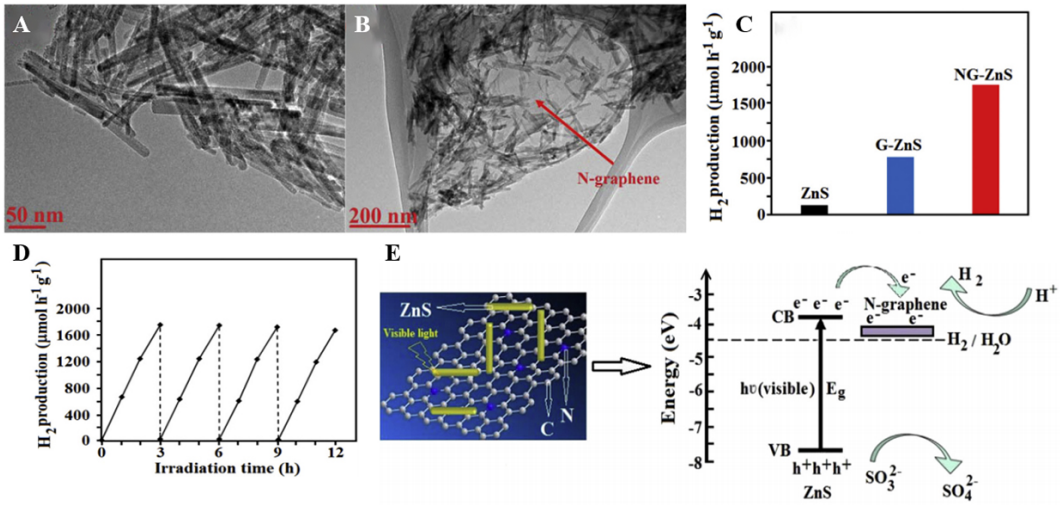


**Figure 9.** (A) High magnification TEM images of pure ZnS nanorods; (B) TEM images of NG-ZnS composite; (C) Comparison of hydrogen production rates on different photocatalysts; (D) Time-cycle photocatalytic hydrogen production over NG-ZnS composite; (E) The energy level diagram for NG-ZnS composite in $Na_2S/Na_2SO_3$ aqueous solution. Copyright 2018, Elsevier[23]. TEM: Transmission electron microscopy; ZnS: Zinc sulfide; NG-ZnS: N-doped graphene-supported ZnS.

Despite the promising photocatalytic properties of ZnS, its wide bandgap and susceptibility to photocorrosion under prolonged illumination limit its practical application. Moon *et al.*[78] tackled these issues by developing N-doped ZnS via ammonia treatment [Figure 10A], enhancing both stability and visible light absorption. The N-doped ZnS demonstrated exceptional stability and sustained hydrogen production under simulated sunlight, with no structural degradation or performance loss after multiple cycles [Figure 10B]. XPS and UV-Vis DRS confirmed improved visible light absorption [Figure 10C-E], while Mott-Schottky and photoelectrochemical tests revealed enhanced charge carrier separation and transport [Figure 10F]. Density Functional Theory (DFT) calculations further supported these results, showing that nitrogen doping raised the VB maximum (VBM) and reduced the oxidative power of holes.

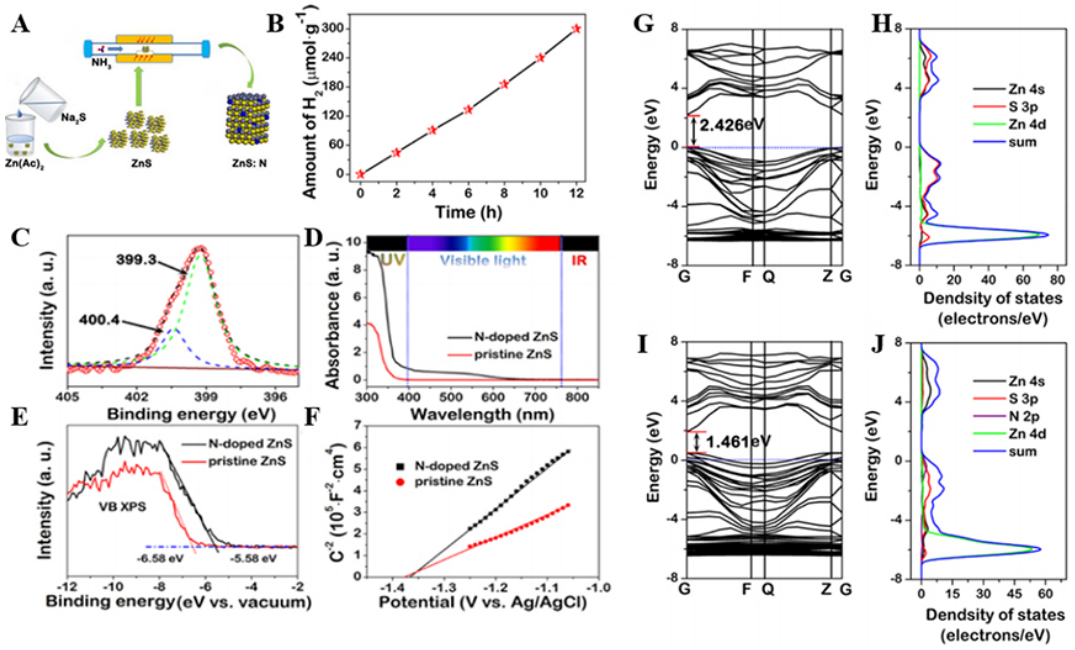


**Figure 10.** (A) Schematic of N-doped ZnS formation via precipitation and nitridation in $NH_3$; (B) Photocatalytic $H_2$ production with 10 vol.% methanol as an electron donor; (C) XPS spectra of N 1s for N-doped ZnS; (D) Vis absorption spectra; (E) Valence-band XPS and (F) Mott-Schottky plots of pristine and N-doped ZnS; Calculated electronic band structure (left) and projected density of states (right) for pristine ZnS (G and H) and N-doped ZnS (I and J). Copyright 2022, Elsevier[78]. ZnS: Zinc sulfide; XPS: X-ray photoelectron spectroscopy; Vis: visible.

This electronic structure adjustment contributed to improved photocatalytic performance under visible light [Figure 10G-J]. These findings highlight the effectiveness of nitrogen doping in addressing the inherent limitations of ZnS, making it a more viable candidate for practical photocatalytic applications.

Xiong *et al.*[24] expanded N-doped ZnS research by synthesizing N-doped ZnS/ZnO composites with a porous plate-like structure using a hydrothermal and in situ transformation method. TEM, HAADF-STEM mapping, and HRTEM confirmed the morphology and structure of the composites [Figure 11A-D], while XRD patterns demonstrated the formation of pure hexagonal ZnS at 500 °C for 5 min [Figure 11E]. XPS spectra identified the oxidation states of Zn, S, O, and N, with N 1s peaks at 399.58, 399.78, and 400.38 eV for ZnS, ZnS/ZnO, and ZnO, respectively, confirming nitrogen doping as the source of visible light activity [Figure 11F-I]. The composite with 6.9 wt.% ZnO achieved the highest hydrogen production rate of 1,790 μmol $h^{-1}$ $g^{-1}$ under visible light ($\lambda > 400$ nm), outperforming pure ZnS and ZnO by seven and 12.3 times, respectively [Figure 11J and K]. This enhancement was attributed to effective charge transfer between ZnS and ZnO, which reduced electron-hole recombination and improved redox efficiency. Additionally, N-doped ZnS/ZnO composites exhibited competitive performance as photoanodes in fuel-sensitized solar cells, highlighting their potential for solar energy conversion and storage. However, a sharp performance decline was observed after the third cycle, attributed to newly adsorbed substances or surface oxide layer formation, which hinder charge carrier transmission and separation. These surface alterations, often irreversible, cause continued performance degradation under prolonged illumination.

Nitrogen doping effectively enhances the photocatalytic performance of ZnS for hydrogen production and pollutant degradation under visible light by improving light absorption, charge carrier separation, and material stability. However, performance variations arise due to differences in preparation methods,

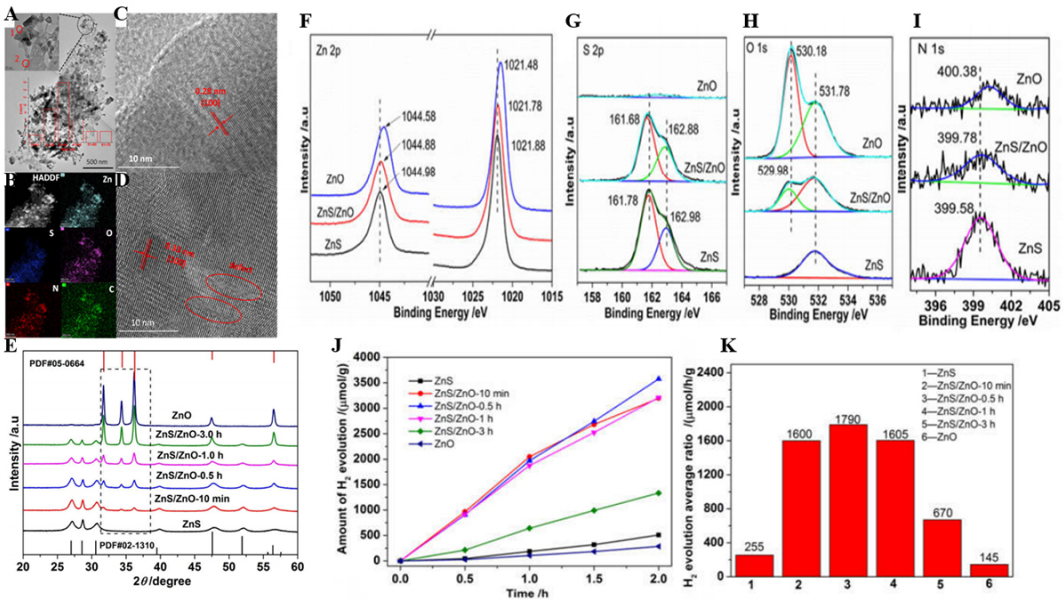


**Figure 11.** (A) TEM and (B) HAADF-STEM with mapping images of ZnS/ZnO-0.5 h; (C and D) HRTEM images at site 1 and site 2 from (A); inset in (A) shows nanoparticle size distribution. (E) XRD patterns of $ZnS(en)_{0.5}$ calcined at 500 °C for 5 min, 10 min, 0.5 h, 1 h, 3 h, and 5 h. XPS spectra: (F) Zn 2p; (G) S 2p; (H) O 1s; and (I) N 1s. ZnS/ZnO-0.5 h denotes the 0.5 h calcined sample; (J) Time-dependent $H_2$ evolution activity and; (K) average $H_2$ evolution rates of the samples. Copyright 2022, MDPI[24]. TEM: Transmission electron microscopy; HAADF-STEM: high-angle annular dark-field scanning transmission electron microscopy; ZnS: Zinc sulfide; HRTEM: high-resolution transmission electron microscopy; XRD: X-ray diffraction.

microstructure, and charge transport efficiency. For example, step-by-step methods such as hydrothermal transformation of ZnS to ZnS/ZnO composites can result in varying nitrogen concentrations and positions compared to simpler one-step solvothermal methods. Microstructural differences, such as nanoporous plate-like morphologies in ZnS/ZnO or ZnS nanorods on N-doped graphene, influence active site availability and electron transport, directly influencing hydrogen production efficiency. Nitrogen doping also narrows the ZnS bandgap, inducing a red shift in light absorption and enhancing visible light utilization. It modifies the electronic structure by raising the VBM, reducing carrier recombination, and increasing charge separation efficiency, as evidenced by lower PL intensity. Optimizing synthesis methods, microstructure, and electronic properties is thus crucial for maximizing the photocatalytic efficiency of N-doped ZnS under visible light.

### Carbon-doped ZnS

Carbon doping in ZnS introduces energy levels within its bandgap, enhancing visible light absorption and photocatalytic activity by modifying its electronic structure. Carbon atoms can either substitute sulfur in the ZnS lattice or form defect states, improving charge carrier separation and migration. This enhancement enables carbon-doped ZnS to effectively drive visible-light photocatalytic reactions, such as water splitting for hydrogen production. Carbon doping is typically achieved through methods such as CVD, hydrothermal synthesis, or heat treatment with carbon sources. Khan *et al.*[44] developed a multi-junction photocatalyst - carbon-doped ZnS-ZnO/Rh nanosheets - with remarkable hydrogen production efficiency under simulated sunlight. ZnS-ZnO nanosheets were synthesized via solvothermal treatment of ZnS in ethylenediamine (EDA) followed by thermal annealing in air, forming ZnO. Carbon, derived from EDA decomposition, acted as the dopant. Rhodium (Rh) was photodeposited in situ, forming a ZnS-ZnO/Rh composite. The catalyst's exceptional performance stemmed from two mechanisms: the Z-scheme heterojunction between ZnS and ZnO, facilitating charge separation and transfer, and the Schottky junction

between Rh and the semiconductor, further enhancing charge separation efficiency. This straightforward synthesis produced high-defect-density photocatalysts ideal for solar energy applications. The study detailed the synthesis of ZnS, ZnS-ZnO, and ZnO, highlighting solvothermal and thermal decomposition methods. Characterization techniques - including field emission-scanning electron microscope (FE-SEM), TEM, XRD, PL, and UV-Vis absorption spectroscopy - provided insights into morphology, crystal structure, optical properties, and composition. Scanning electron microscope (SEM) and TEM images [Figure 12A-C] revealed the nanosheet morphology, while photocurrent density and photocatalytic activity measurements confirmed enhanced $H_2$ generation. XRD patterns and optical properties demonstrated the impact of carbon doping on activity. DFT-based calculations [Figure 12D and E] supported the energy preferences of carbon doping and its role in charge separation. ZnS-ZnO achieved significantly higher $H_2$ production from $Na_2S/Na_2SO_3$ solution than pure ZnS and ZnO, as summarized in Figure 12F-H. This improvement was attributed to enhanced charge separation, corroborated by experimental and computational findings.

### Carbon and nitrogen Co-doped ZnS

C and N co-doping in ZnS photocatalysts significantly enhances photocatalytic activity by reducing the bandgap and improving visible light absorption. Co-doping introduces defect states within the bandgap, facilitating efficient charge carrier separation and reducing recombination rates, which is critical for processes such as hydrogen generation and pollutant degradation. Additionally, it improves surface reactivity, enhancing interactions with water molecules and substrates. Moon *et al.*[78] developed highly efficient, durable ZnS photocatalysts for hydrogen production using zinc vacancies and C, N co-doping. ZnS nanoparticles (< 10 nm) were synthesized via a hydrothermal method using two sulfur sources: sulfur powder (ZnS-S) and thiourea (ZnS-thio) [Figure 13A and B]. ZnS-S exhibited a higher concentration of zinc vacancies, while ZnS-thio was further co-doped with C and N to enhance photocatalytic performance. C, N co-doped ZnS-thio nanoparticles showed superior photocatalytic hydrogen production (176 $\mu mol\ g^{-1}\ h^{-1}$) without sacrificial agents [Figure 13C], twice as effective as ZnS-S due to higher generation of hydroxyl and superoxide radicals. UV-Vis spectra confirmed a red shift in the absorption spectrum [Figure 13D], while PL studies showed lower PL intensity, indicating reduced charge recombination [Figure 13E]. Zinc vacancies and co-doping synergistically reduced the bandgap, enhanced charge separation, and improved visible light absorption. These photocatalysts also demonstrated excellent stability, maintaining hydrogen production efficiency over five cycles without photocorrosion. The durability was attributed to zinc vacancies and C, N co-doping, which protected the catalyst from degradation. Additionally, co-doping lowered the surface energy of ZnS-thio, favoring the growth of smaller nanoparticles (5.78 nm) compared to ZnS-S (6.84 nm). Lower surface energy, driven by doping-induced changes in atomic arrangement, promotes stable crystal growth during synthesis. This study highlights the advantages of C, N co-doped ZnS photocatalysts: enhanced visible light absorption, efficient charge separation, excellent photostability, and favorable crystal growth, making them promising for hydrogen production and environmental applications.

To address the issues of low solar energy utilization, fast charge recombination, and photocorrosion in photocatalysts, Wu *et al.*[27] synthesized N-doped carbon quantum dots (NCQDs) via hydrothermal treatment and combined them with ZnS to prepare NCQDs/ZnS nanocomposites. XRD analysis revealed three main diffraction peaks of ZnS at 28.8°, 47.9°, and 56.9°, corresponding to the (111), (220), and (311) planes of cubic-phase ZnS. No NCQD peaks were observed due to their low content, high dispersion, and amorphous nature. With increasing NCQD content, ZnS peaks broadened, indicating reduced nanoparticle size, lattice distortion, and defects [Figure 14A]. TEM and SEM images showed ZnS particle sizes around 200 nm, while the NCQDs/ZnS composite particles were smaller (< 100 nm). HRTEM confirmed lattice spacings of 0.31 and 0.22 nm, corresponding to the (111) plane of ZnS and the (100) plane of graphitic carbon, respectively, verifying successful NCQD loading on ZnS [Figure 14B and C]. XPS analysis revealed

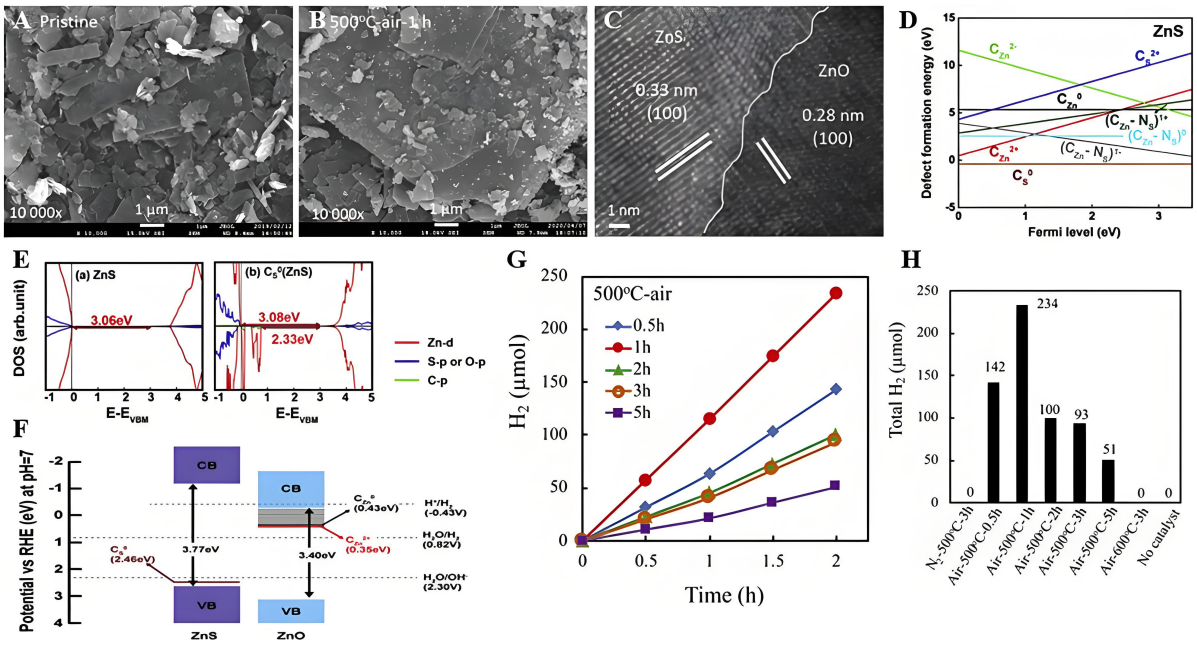


**Figure 12.** (A and B) SEM images of the pristine and 500 °C-air-1 h treated samples; (C) HRTEM image of the 500 °C-air-1 h sample; (D) Defect formation energies in ZnS *vs.* Fermi level for CZn, CS, CO, and $C_{Zn}$-Ns/$C_{Zn}$-NO defects; (E) Density of states for defect-free ZnS: Zn d-states (red), S/O p-states (blue), and C p-states (green); (F) Band alignment of ZnS and ZnO defects *vs.* RHE at pH 7 (band gaps: ZnS, 3.77 eV; ZnO, 3.40 eV), showing $CS^0$ (ZnS), $CZn^0$ (ZnO), and $C_2$ + Zn (ZnO) defect levels. (G) $H_2$ generation time course under UV light with $Na_2S/Na_2SO_3$ as donors, and (H) total $H_2$ produced. Copyright 2021, Elsevier[44]. SEM: Scanning electron microscope; HRTEM: high-resolution transmission electron microscopy; UV: ultraviolet.

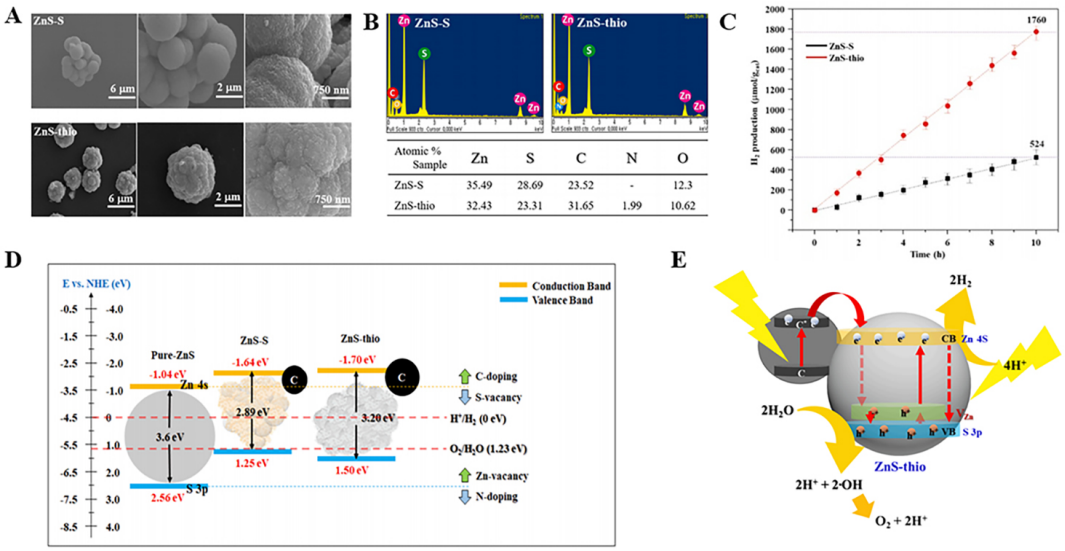


**Figure 13.** (A) SEM images. (B) EDS patterns. (V) $H_2$ gas generated from water-splitting without any sacrificial agent for 10 h over ZnS-S and ZnS-thio particles. (D) Energy position diagrams for the ZnS-S and ZnS-thio particles. (E) Hydrogen evolution and charge transfer mechanisms over the defective ZnS-thio catalyst. Copyright 2022, Elsevier[78]. SEM: Scanning electron microscope; EDS: energy dispersive X-ray specctroscopy; ZnS: Zinc sulfide.

N 1s peaks at 399.9 and 401.4 eV in NCQDs, assigned to pyrroline and graphite N-C3. In NCQDs/ZnS, N 1s peaks shifted to 399.3 and 401.4 eV, suggesting a strong interaction between NCQDs and ZnS. C 1s spectra

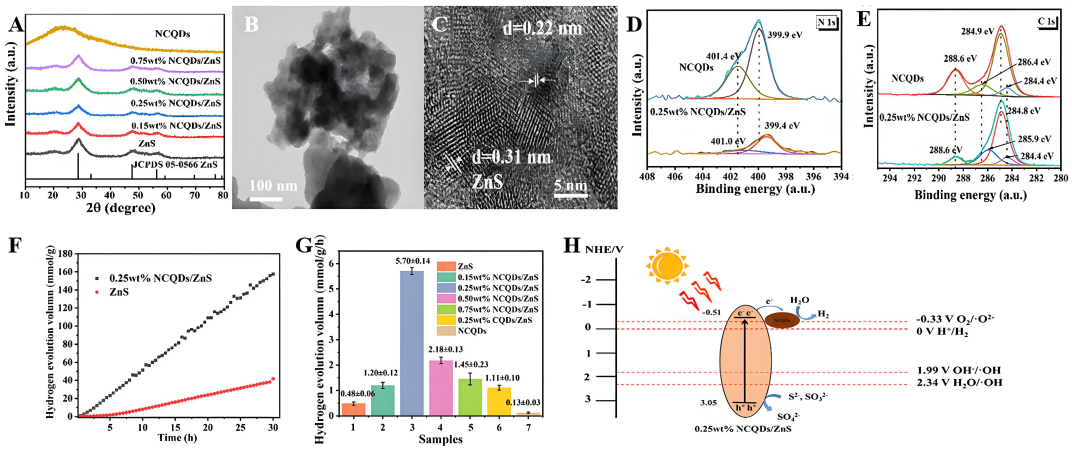


**Figure 14.** (A) XRD patterns of NCQDs, ZnS, and NCQD-modified ZnS. TEM images of (B) 0.25 wt.% NCQDs/ZnS and (C) its HRTEM. XPS spectra of NCQDs and 0.25 wt.% NCQDs/ZnS: (D) N 1s and (E) C 1s; (F) Catalytic stability of 0.25 wt.% NCQDs/ZnS and ZnS under full-spectrum irradiation (30 h, Xe lamp, 230 mW $cm^{-2}$). (G) Photocatalytic hydrogen evolution for ZnS, NCQDs, and NCQDs/ZnS with varying NCQDs content. (H) Proposed hydrogen production mechanism on NCQDs/ZnS. Copyright 2024, American Chemical Society[27]. XRD: X-ray diffraction; NCQD: N-doped carbon quantum dot; ZnS: Zinc sulfide; TEM: transmission electron microscopy; HRTEM: high-resolution transmission electron microscopy; XPS: X-ray photoelectron spectroscopy.

showed peaks for C-C, C-O, and C-N bonds [Figure 14D and E]. The optimized 0.25 wt.% NCQDs/ZnS catalyst achieved a hydrogen production rate of 5.70 mmol $g^{-1}$ $h^{-1}$ under full-spectrum irradiation, which was 11.88, 43.84, and 5.14 times higher than that of ZnS, NCQDs, and CQDs/ZnS, respectively. The catalyst demonstrated excellent stability, as NCQDs effectively mitigated ZnS photocorrosion and oxidation [Figure 14F and G]. The enhanced photocatalytic performance was attributed to NCQDs, which improved charge separation, optimized material structure, and increased specific surface area. Mott-Schottky analysis, UV-Vis DRS, and EPR confirmed these findings, and a possible reaction mechanism was proposed [Figure 14H]. This study highlights NCQD-modified ZnS as a promising strategy for enhancing ZnS-based photocatalysts for hydrogen production.

Mani *et al.*[29] employed a novel one-step solution combustion synthesis method to prepare C, N co-doped ZnS nanomaterials with visible-light activity. This surfactant-free method, which also avoided inert gas atmospheres, produced rice-shaped ZnS nanoparticles with enhanced photocatalytic properties. TEM and XRD confirmed the nanoscale size and hexagonal phase of the particles [Figure 15A-E], while diffuse reflectance UV-Vis spectroscopy revealed a red shift in absorption due to C, N co-doping. The study also examined the effect of pH on photocatalytic activity. Under acidic conditions (pH < 2), Cr(VI) reduction reached 100% within 15 min [Figure 15F], while alkaline conditions favored methylene blue (MB) oxidation. The enhanced photocatalytic activity was attributed to improved electron transfer efficiency, facilitated by the lower surface energy of C, N-doped ZnS. This promotes rapid electron-hole separation and migration, boosting both pollutant degradation and hydrogen production performance. XPS and elemental analysis further confirmed the incorporation of C and N into the ZnS lattice [Figure 15G-J]. By optimizing the metal-to-sulfur precursor ratio, the ZnS(1: 5) sample achieved a remarkable hydrogen production rate of 10,000 μmol/h/g under visible light [Figure 15K].

### Doping ZnS with other elements

Beyond C and N, other elements have been explored to enhance ZnS photocatalytic performance. Xu *et al.*[25] investigated anion-cation co-doping to engineer the ZnS(110) surface for improved visible light responsiveness and water-splitting activity. Figure 16A provides a basis for the subsequent study of the

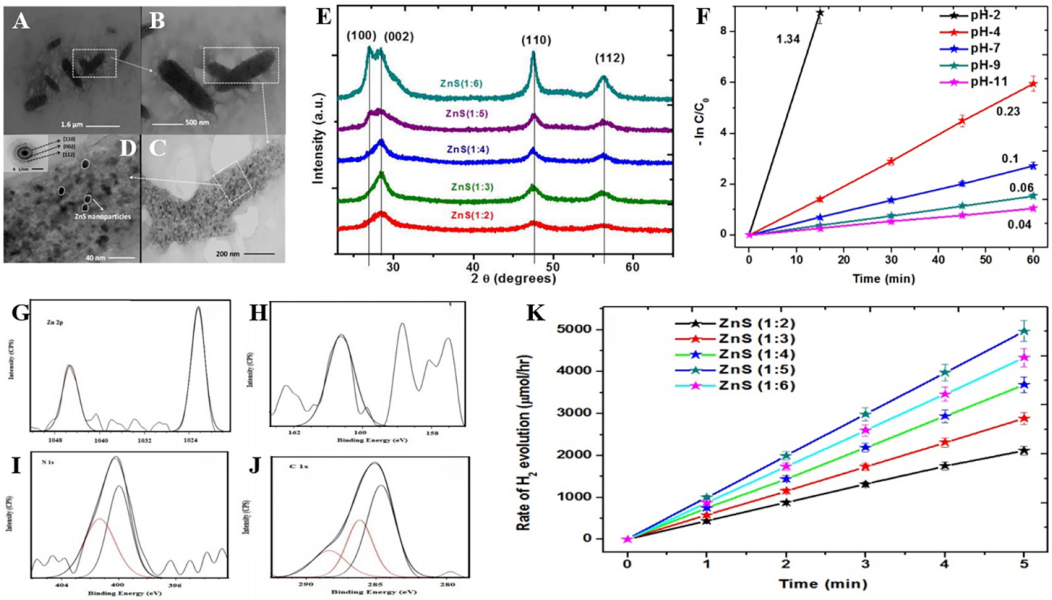


**Figure 15.** (A) TEM image of ZnS rice grain microstructures; (B-D) Enlarged views showing ZnS nanoparticles; (D, inset) selected area diffraction pattern; (E) Powder XRD patterns of combustion-synthesized ZnS; (F) Effect of pH on Cr(VI) photocatalytic reduction ($C_0$ = 10 ppm, catalyst = 100 mg, pH = 2, 4, 7, 9, 11); XPS spectra of (G) Zn 2p; (H) S 2p; (I) N 1s; and (J) C 1s core levels; (K) $H_2$ evolution rates from water with 1M $Na_2S$ and 1M $Na_2SO_3$ sacrificial agents over 5 h for all ZnS samples. Copyright 2014, Royal Society of Chemistry[29]. TEM: Transmission electron microscopy; ZnS: Zinc sulfide; XRD: X-ray diffraction.

changes in the band structure under various doping conditions by showing the band structure and density of state distribution of the pure ZnS (110) surface. Using mixed density functional theory (DFT), they analyzed the effects of single dopants - Ru, C, N, and F - and co-dopants such as (Ru + C), (Ru + N), and (Ru + F) on the band structure [Figure 16B-E]. Single dopants partially reduced the ZnS(110) bandgap but introduced undesirable unoccupied states, hindering water oxidation-reduction reactions. In contrast, (Ru + C) co-doping lowered the bandgap to 2.37 eV, enhanced visible light absorption, and aligned the band edge positions with water oxidation-reduction potentials [Figure 16F-I]. This configuration facilitated charge separation and provided sufficient driving force for hydrogen production. Moreover, (Ru + C) co-doping improved thermodynamic stability by reducing formation energy and enhancing solubility [Figure 16J-L]. These findings highlight (Ru + C)-co-doped ZnS(110) as a promising photocatalyst for solar-driven hydrogen production.

Anion substitution significantly influences the electronic structure and properties of materials compared to cation substitution [Figure 17A and B]. To investigate this, first-principles DFT calculations were conducted to study the effects of P and Cl substitution on hexagonal and cubic CdS and ZnS[80]. Using the Quantum ESPRESSO package with plane-wave basis sets and pseudopotential methods, the study employed the generalized gradient approximation Perdew-Burke-Ernzerhof and local density approximation Perdew-Zunger functionals, while hybrid (HSE) functionals were used to estimate bandgaps. The results, supported by both theoretical predictions and experimental validation, demonstrated that P and Cl co-substitution is feasible and effectively reduces the bandgap [Figure 17C and D]. XPS confirmed successful P and Cl doping. In CdS, P acts as a p-type dopant and Cl as an n-type dopant, reducing the bandgap from 2.3 eV to 1.8 eV. Similarly, co-substitution in ZnS reduced the bandgap from 3.5 eV to 2.8 eV [Figure 17E-J]. UV-Vis absorption spectra revealed a redshift in the absorption edge, corroborating the bandgap reduction [Figure 17K-N]. Preliminary photocatalytic hydrogen production tests indicated that P, Cl co-doped CdS exhibited enhanced activity compared to pristine CdS [Figure 17O]. These findings highlight anion co-

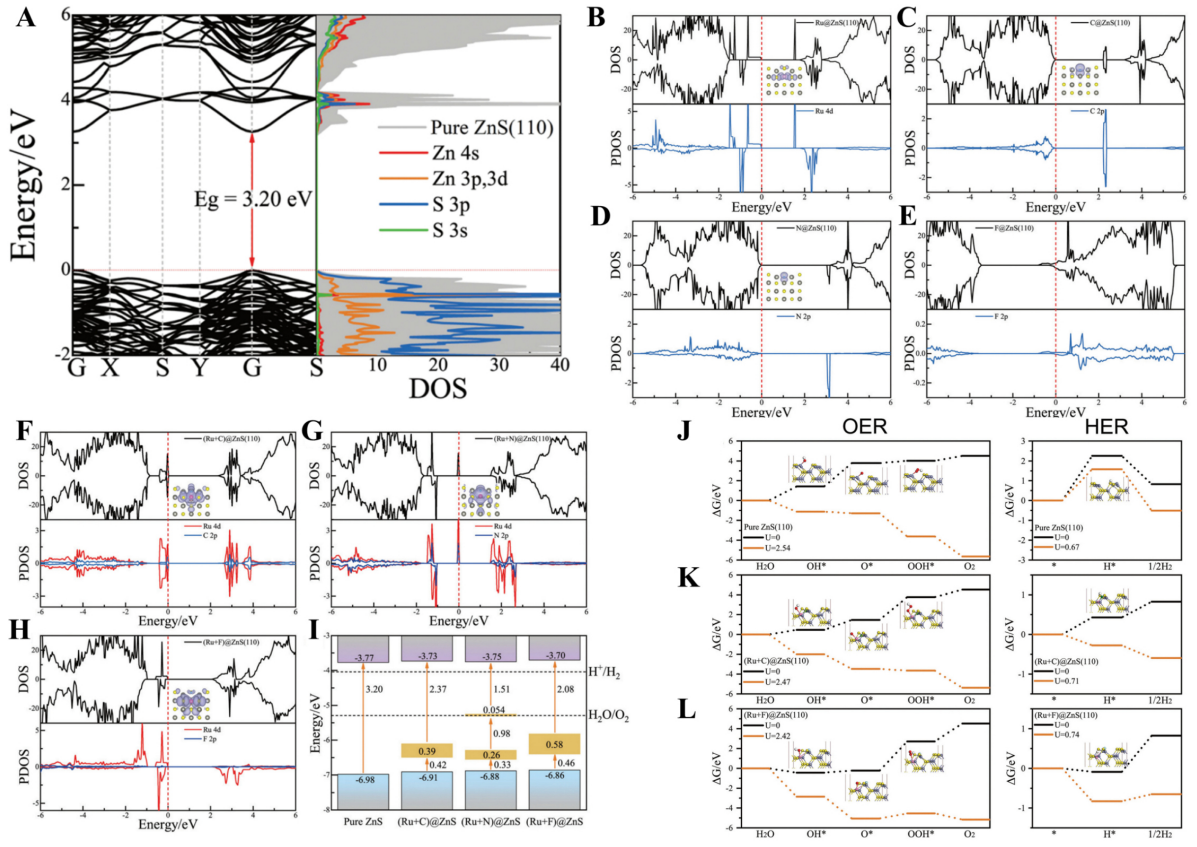


**Figure 16.** (A) HSE06-calculated band structure and projected DOS of pure ZnS(110) surface; dashed line shows the Fermi level. HSE06 total and partial DOS of (B) Ru-; (C) C-; (D) N-; and (E) F-monodoped ZnS(110) surfaces with impurity state distributions (insets). HSE06 total and partial DOS of (F) (Ru + C)-, (G) (Ru + N)-, and (H) (Ru + F)-co-doped ZnS(110) surfaces with impurity state distributions (insets). (I) Band edge positions of pure and co-doped ZnS(110) surfaces relative to the vacuum scale; water redox potentials at pH = 7 are shown (red dashed lines). Gibbs free energy profiles for OER (left) and HER (right) on (J) pure, (K) (Ru + C)-, and (L) (Ru + F)-co-doped ZnS(110) surfaces, with and without external potentials (orange and black lines). Insets show favorable adsorption intermediates. Copyright 2014, Royal Society of Chemistry[25]. HSE06: A hybrid functional theory; DOS: density of states; ZnS: Zinc sulfide; OER: oxygen evolution reaction; HER: hydrogen evolution reaction.

substitution as an effective strategy to modify the electronic structure and optical properties of CdS and ZnS, particularly through bandgap reduction, thereby improving their photocatalytic performance.

Researchers have modified the particle size, surface area, and defects of ZnS through doping and defect engineering. Moon *et al.*[79] synthesized C, N, O co-doped ZnS particles with Zn and S defects using EDA derivatives as capping agents. These agents controlled particle shape and optical properties by forming stable cyclic structures with metal ions. The resulting ZnS particles exhibited a mix of cubic and hexagonal phases, characterized by XRD, SEM, and TEM. PL spectra, time-resolved PL, and photoelectric current tests assessed the photocatalytic activity. Doping and defect introduction significantly influenced the bandgap and photocatalytic performance. As shown in Figure 18A, ZnS-none exhibited a reduced bandgap compared to pure non-defective ZnS (3.6 eV), with the VBM shifted upward by O- and S-doping. ZnS particles with capping agents showed slightly larger bandgaps than ZnS-none but were still reduced compared to pure ZnS. ZnS-en and ZnS-trien, with high O and N-doping, showed a larger VBM shift. ZnS-en particles excelled in hydrogen production during water splitting, producing 2547 μmol $g^{-1}$ of hydrogen over 10 h [Figure 18B], outperforming other samples. This improvement is attributed to Zn and S defects

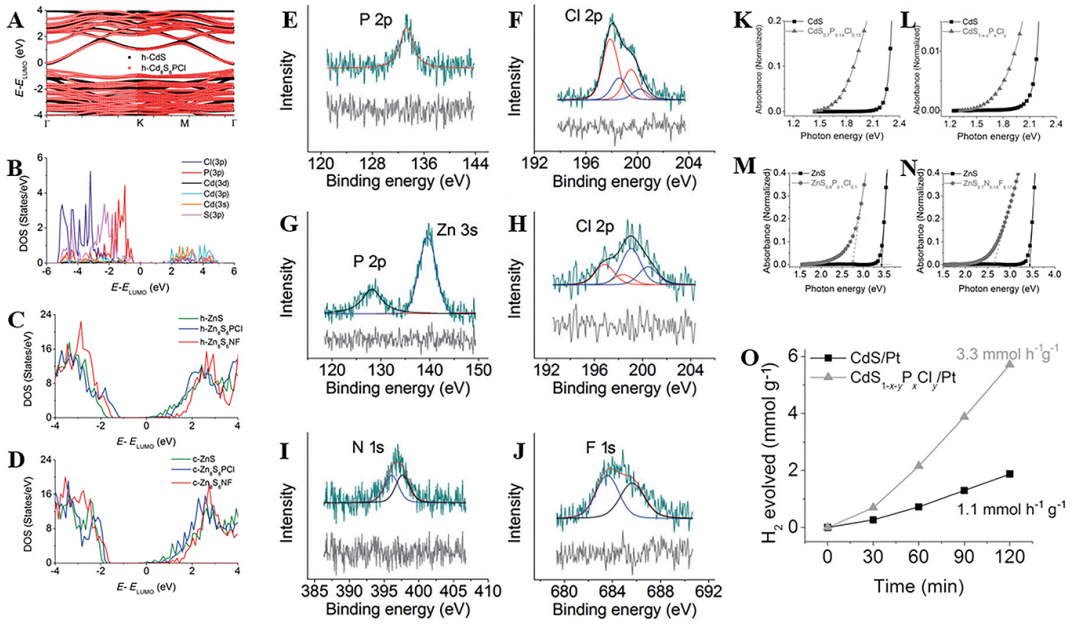


**Figure 17.** (A) Electronic structure and; (B) projected density of states of h-$Cd_8S_6PCl$ show an isolated band from P 3p-orbitals at the top of the valence band. Comparison of the density of states for $Zn_8S_6AB$ and pristine ZnS in (C) hexagonal and; (D) cubic structures. High-resolution XPS spectra: (E) P 2p and; (F) Cl 2p in P, Cl-substituted CdS; (G) P 2p and; (H) Cl 2p in P, Cl-substituted ZnS; (I) N 1s and; (J) F 1s in N, F co-substituted ZnS; (K, L) Electronic absorption spectra of pristine CdS *vs.* P, Cl co-doped CdS prepared by two methods. Comparison of absorption spectra: (M) P, Cl-substituted ZnS and; (N) N, F-substituted ZnS; (O) Visible-light-induced hydrogen evolution by CdS/Pt and $CdS_{1-x-y}P_xCl_y$/Pt over time in $Na_2S$-$Na_2SO_3$. Copyright 2015, Wiley Online Library[80]. ZnS: Zinc sulfide; XPS: X-ray photoelectron spectroscopy.

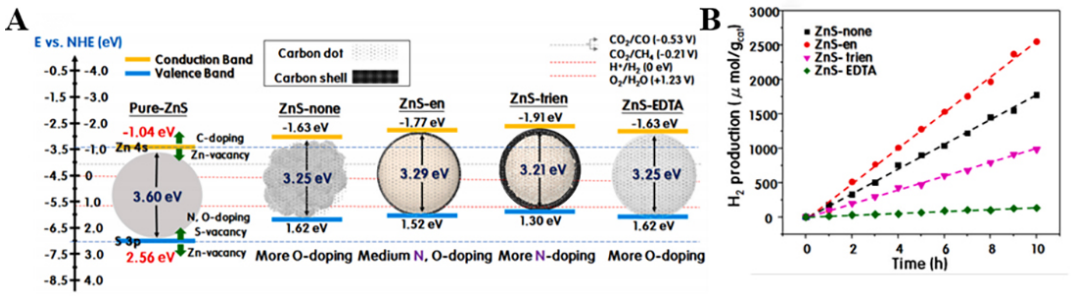


**Figure 18.** (A) Energy diagrams. (B) $H_2$ production by water splitting. Copyright 2023, Elsevier[79].

and C, N, O co-doping, which enhance charge separation. Although ZnS-trien performed less effectively in water splitting, it demonstrated excellent stability in $CO_2$ reduction, with a $CO_2$ conversion efficiency 14 times higher than ZnS-none, highlighting its potential for $CO_2$ photoreduction. The study suggests that in ZnS-en, carbon dots (CDs) on the particle surface act as electron reservoirs, enhancing water adsorption and hydrogen production. In ZnS-trien, N-CDs attract electrons, improving $CO_2$ reduction. Both ZnS-en and ZnS-trien showed stability over multiple cycles, with ZnS-en maintaining good hydrogen production and ZnS-trien performing stably in $CO_2$ reduction. These findings demonstrate that C, N, O co-doping and defects can significantly enhance ZnS's photocatalytic performance, offering new strategies for stable, cost-effective photocatalysts. The reduced surface energy of co-doped ZnS enhances its adsorption of reactant molecules, improving catalytic efficiency.

### The differences of ZnS doped with different non-metal elements

Doping ZnS with non-metal elements such as N, C, and others has been extensively studied to enhance its photocatalytic performance, particularly in the visible light region. Nitrogen doping introduces impurity levels within the bandgap, reducing the energy required to excite electrons and enabling absorption of visible light, which is crucial for solar energy applications[81]. Carbon doping creates additional energy levels within the bandgap, enhancing visible light absorption and photocatalytic activity, with carbon atoms potentially substituting sulfur atoms in the ZnS lattice or forming carbon-related defect states[82]. Co-doping with carbon and nitrogen improves visible light absorption and charge carrier separation, reducing the bandgap and introducing defect states that facilitate charge carrier separation[83]. Other non-metal dopants such as F, P, and chlorine (Cl) also lower the bandgap, enhancing photocatalytic performance[83]. Each dopant alters the electronic structure, bandgap, and photocatalytic activity of ZnS, enhancing visible light absorption and the efficiency of charge carrier separation, which are critical for improving the photocatalytic performance of ZnS in applications such as hydrogen production and environmental remediation.

## CHALLENGES AND FUTURE OUTLOOK

### Challenges and limitations

Non-metal doping of ZnS shows significant promise for enhancing photocatalytic performance, particularly in water splitting applications, but several critical challenges and limitations remain:

(1) Catalyst stability and material degradation: A major challenge for photocatalysts during hydrogen production is maintaining structural and chemical stability over extended periods. Non-metal doping can sometimes compromise the stability of ZnS during photocatalytic reactions due to defects, surface modifications, or excessive lattice distortion. This instability can lead to photocorrosion, reduced activity, and material degradation, especially under prolonged light irradiation or in aqueous environments[29,44]. Therefore, achieving durable performance remains a crucial issue.

(2) Doping level control: The photocatalytic activity of non-metal doped ZnS strongly depends on the doping concentration. While low levels of doping can improve charge separation and extend light absorption, excessive doping often results in lattice defects, carrier recombination, and reduced catalytic efficiency. Maintaining an optimal doping level remains challenging, as uncontrolled synthesis processes may lead to non-uniform doping or insufficient dopant incorporation into the ZnS lattice[84].

(3) High synthesis temperatures and energy costs: Current synthesis methods for non-metal doped ZnS often require high temperatures and extended reaction times, which are energy-intensive and costly. These conditions can hinder precise doping control and limit the formation of the desired crystal phases. Moreover, phase transitions between sphalerite and wurtzite structures, induced by non-metal doping, can unpredictably influence the electronic structure and photocatalytic properties of ZnS.

(4) Limited reactivity and surface optimization: Effective photocatalytic hydrogen production requires materials with large surface areas, abundant active sites, and efficient charge separation. Non-metal doping may alter the surface properties of ZnS, influencing reactant adsorption, reaction pathways, and product generation. However, achieving a balance between charge separation and recombination remains challenging, and further surface optimization strategies are required.

(5) Environmental and scalability concerns: The use of toxic or hazardous precursors during synthesis poses environmental and safety challenges. Moreover, the scalability of non-metal doped ZnS production remains

limited due to cost, synthesis complexity, and inefficiencies in achieving uniform and reproducible doping on a large scale.

### Solutions and future research directions

To overcome these challenges and advance the application of non-metal doped ZnS for photocatalytic water splitting, the following strategies and research directions are proposed:

(1) Development of innovative synthesis methods: New synthesis approaches, such as hydrothermal synthesis, CVD, and microwave-assisted techniques, can produce non-metal doped ZnS with tailored morphologies, crystal structures, and controlled doping levels at lower energy costs. Additionally, methods such as vapor-phase ion exchange allow precise control of dopant concentration and distribution while minimizing solvent interference. Optimizing synthesis parameters, such as temperature, reaction time, and dopant precursor concentration, can ensure improved material uniformity, stability, and efficiency[85].

(2) Stability enhancement and surface engineering: Enhancing the stability of doped ZnS during photocatalytic reactions is essential. This can be achieved through surface passivation techniques, core-shell structures, and protective coatings that minimize photocorrosion while preserving photocatalytic activity. Additionally, coupling doped ZnS with noble metal nanoparticles (e.g., Pt, Au, or Ag) can act as cocatalysts to enhance electron capture, reduce charge recombination, and improve hydrogen evolution efficiency. Careful optimization of noble metal deposition amounts is necessary to balance costs and performance[86-88].

(3) Optimization of doping levels and structures: Achieving optimal dopant concentration is critical for maximizing performance. Detailed investigations, such as thermogravimetric analysis and temperature-gradient experiments, can help identify appropriate doping temperatures and durations. Beyond traditional non-metal dopants (e.g., carbon and nitrogen), exploring halogen doping (e.g., chlorine and fluorine) and co-doping strategies with other elements can unlock further improvements in charge transport, bandgap narrowing, and light absorption. Structural engineering, including the development of one- (1D) and two-dimensional (2D) ZnS materials, also holds promise for enhancing photocatalytic properties.

(4) Improvement of charge separation efficiency: Enhancing charge separation while minimizing electron-hole recombination remains a primary goal for efficient water splitting. Strategies such as constructing heterojunctions with other semiconductors, introducing oxygen vacancies or sulfur defects, and employing plasmonic nanostructures can improve charge dynamics and extend light absorption into the visible range. These approaches can be further validated using computational simulations to predict electronic structure changes and guide experimental designs.

(5) Environmental and cost considerations: To address environmental concerns and improve scalability, future research should focus on using green and non-toxic precursors in synthesis processes. Reducing energy consumption through low-temperature or energy-efficient synthesis methods (e.g., microwave or sonochemical techniques) can significantly lower costs and improve sustainability. Moreover, enhancing synthesis reproducibility and scalability will be critical for real-world applications.

(6) Broader applications and interdisciplinary research: Beyond hydrogen production, doped ZnS materials hold significant potential in addressing various environmental and energy challenges. For instance, they can be applied in water treatment to degrade organic pollutants such as pesticides, dyes, and volatile organic compounds (VOCs) under UV and visible light irradiation. Additionally, doped ZnS can facilitate carbon dioxide reduction, converting $CO_2$ into valuable chemicals such as methane and methanol, thereby

contributing to carbon neutrality goals. In air purification, these photocatalysts efficiently remove harmful air pollutants, showcasing their versatility and promise for sustainable environmental remediation and energy applications[89-92].

Interdisciplinary collaboration among materials scientists, chemists, and engineers will be essential to fully exploit the potential of doped ZnS for clean energy and environmental remediation. Future studies should focus on uncovering the mechanisms by which different non-metal dopants influence the electronic structure, charge dynamics, and photocatalytic efficiency of ZnS, providing a theoretical basis for the rational design of high-performance materials.

## CONCLUSION

Non-metal doped ZnS nanostructures have demonstrated significant potential in photocatalytic hydrogen production and environmental remediation. Non-metal elements such as nitrogen and carbon effectively address ZnS's wide bandgap and rapid recombination of photogenerated carriers, enhancing photocatalytic performance. For example, nitrogen doping introduces impurity energy levels for visible light absorption, while carbon doping generates additional energy states, improving light absorption and charge separation. Nitrogen-carbon co-doping suppresses electron-hole recombination by creating defect states and facilitating charge migration, while certain dopants reduce lattice defects and improve stability. NCQDs/ZnS achieves the highest hydrogen production rate of 5,700 μmol $g^{-1}$ $h^{-1}$ due to the high electron affinity of NCQDs, promoting charge separation and suppressing recombination. The increased surface area further enhances active sites and reaction pathways. Beyond hydrogen production, non-metal doped ZnS efficiently degrades pollutants, showing potential for environmental cleanup. The introduction of reaction aids broadens light absorption and improves charge carrier separation, boosting hydrogen evolution during water splitting. Despite these advancements, challenges remain for large-scale industrial applications, necessitating further research into material optimization and scalability.

## DECLARATIONS

### Authors' contributions

Reviewed literature extensively, wrote and modified articles, created figures, and set the layout: Wang, S.
Polished the article and designed the figures: Niu, X.; Wang, L.
Revised the article, provided research direction, and offered funding support: Bi, J.; Yang, W.; Hou, H.

### Financial support and sponsorship

This work was supported by the Natural Science Foundation of Zhejiang Province (Grant No. LY23E020002), National Natural Science Foundation of China (NSFC, Grant No. 52272085), and Ningbo Youth Science and Technology Innovation Leading Talents Project (Grant No. 2023QL031).

### Availability of data and materials

Not applicable.

### Conflicts of interest

All authors declared that there are no conflicts of interest.

### Ethical approval and consent to participate

Not applicable.

### Consent for publication

Not applicable.



## REFERENCES

1. Yuan, Z.; Zhu, X.; Jiang, Z. Recent advances of constructing metal/semiconductor catalysts designing for photocatalytic $CO_2$ hydrogenation. *Molecules* **2023**, *28*, 5693. DOI PubMed PMC
2. Ulukardesler, A. H. Biodiesel production from waste cooking oil using different types of catalysts. *Processes* **2023**, *11*, 2035. DOI
3. Caglar, A. E.; Daştan, M.; Avci, S. B.; Ahmed, Z.; Gönenç, S. Modeling the influence of mineral rents and low-carbon energy on environmental quality: new insights from a sustainability perspective. *Nat. Resour. Forum.* **2024**, *48*, 1456-76. DOI
4. Ju, Y.; Nie, X.; Zhu, Y.; Xie, H. *In situ* fluidized mining and conversion solution to alleviate geological damage and greenhouse gas emissions due to coal exploitation: a numerical analysis and evaluation. *Energy. Sci. . Eng.* **2021**, *9*, 40-57. DOI
5. Gitelman, L.; Magaril, E.; Kozhevnikov, M. Energy security: new threats and solutions. *Energies* **2023**, *16*, 2869. DOI
6. Fajardy, M.; Mac, D. N. The energy return on investment of BECCS: is BECCS a threat to energy security? *Energy. Environ. Sci.* **2018**, *11*, 1581-94. DOI
7. Leonzio, G.; Chachuat, B.; Shah, N. Towards ethylene production from carbon dioxide: economic and global warming potential assessment. *Sustain. Prod. Consump.* **2023**, *43*, 124-39. DOI
8. Li, Y.; Zhu, F.; Liu, E.; et al. Carbon dioxide capture and green conversion to clean energy against global warming. *Adv. Compos. Hybrid. Mater.* **2024**, *7*, 955. DOI
9. Tang, J.; Ni, H.; Peng, R.; Wang, N.; Zuo, L. A review on energy conversion using hybrid photovoltaic and thermoelectric systems. *J. Power. Sources.* **2023**, *562*, 232785. DOI
10. Mondal, S.; Mondal, A.; Rathore, J.; Koundinya, K. K.; Sharma, A. K. India's shift toward sustainable energy: a comprehensive approach to renewable energy integration and environmental sustainability. *J. Renew. Sustain. Ener.* **2024**, *16*, 042701. DOI
11. Ye, Z.; Zheng, R.; Li, S.; et al. A review: recent advances of piezoelectric photocatalysis in the environmental fields. *Nanomaterials. (Basel).* **2024**, *14*, 1641. DOI PubMed PMC
12. Li, C. F.; Pan, W. G.; Zhang, Z. R.; Wu, T.; Guo, R. T. Recent progress of single-atom photocatalysts applied in energy conversion and environmental protection. *Small* **2023**, *19*, e2300460. DOI PubMed
13. Chengli, Z.; Ronghua, M.; Qi, W.; Mingrui, Y.; Rui, C.; Xiaonan, Z. Photocatalytic degradation of organic pollutants in wastewater by heteropolyacids: a review. *J. Coord. Chem.* **2021**, *74*, 1751-64. DOI
14. Dong, S.; Gong, Y.; Zeng, Z.; et al. Dissolved organic matter promotes photocatalytic degradation of refractory organic pollutants in water by forming hydrogen bonding with photocatalyst. *Water. Res.* **2023**, *242*, 120297. DOI
15. Li, T.; Wang, P.; He, M.; Zhang, T.; Yang, C.; Li, Z. Metal-organic frameworks for photocatalytical carbon dioxide reduction reaction. *Coord. Chem. Rev.* **2024**, *521*, 216179. DOI
16. Kandy M, Rajeev K A, Sankaralingam M. Development of proficient photocatalytic systems for enhanced photocatalytic reduction of carbon dioxide. *Sustain. Energy. Fuels.* **2021**, *5*, 12-33. DOI
17. Ekspong, J.; Larsen, C.; Stenberg, J.; et al. Solar-driven water splitting at 13.8% solar-to-hydrogen efficiency by an earth-abundant electrolyzer. *ACS. Sustain. Chem. Eng.* **2021**, *9*, 14070-8. DOI
18. Li, R.; Luan, J.; Zhang, Y.; et al. A review of efficient photocatalytic water splitting for hydrogen production. *Renew. Sustain. Energy. Rev.* **2024**, *206*, 114863. DOI
19. Yuan, L.; Han, C.; Yang, M.; Xu, Y. Photocatalytic water splitting for solar hydrogen generation: fundamentals and recent advancements. *Int. Rev. Phys. Chem.* **2016**, *35*, 1-36. DOI
20. Madkour, M.; Al Sagheer, F. Au/ZnS and Ag/ZnS nanoheterostructures as regenerated nanophotocatalysts for photocatalytic degradation of organic dyes. *Opt. Mater. Express.* **2017**, *7*, 158. DOI
21. Chankhanittha, T.; Watcharakitti, J.; Piyavarakorn, V.; et al. ZnO/ZnS photocatalyst from thermal treatment of ZnS: influence of calcination temperature on development of heterojunction structure and photocatalytic performance. *J. Phys. Chem. Solids.* **2023**, *179*, 111393. DOI
22. Zhang, K.; Xu, Y.; Liu, F.; Yan, G.; Guo, S. Preparation and properties of ZnS-CdSe@Co/N-C core/shell composites for visible light photoconversion of $CO_2$. *New. J. Chem.* **2023**, *47*, 12550-3. DOI
23. Azarang, M.; Sookhakian, M.; Aliahmad, M.; et al. Nitrogen-doped graphene-supported zinc sulfide nanorods as efficient Pt-free for visible-light photocatalytic hydrogen production. *Int. J. of. Hydrog. Energy.* **2018**, *43*, 14905-14. DOI
24. Xiong, J.; Wang, X.; Wu, J.; Han, J.; Lan, Z.; Fan, J. *In situ* fabrication of n-doped Zns/Zno composition for enhanced visible-light photocatalytic $H_2$ evolution activity. *Molecules* **2022**, *27*, 8544. DOI PubMed PMC
25. Xu, L.; Meng, J.; Wang, J.; Wang, L.; Li, Q. Hybrid density functional study on band structure engineering of ZnS(110) surface by anion-cation codoping for overall water splitting. *New. J. Chem.* **2022**, *46*, 8079-87. DOI
26. Tie, L.; Sun, R.; Jiang, H.; et al. Facile fabrication of N-doped ZnS nanomaterials for efficient photocatalytic performance of organic

pollutant removal and $H_2$ production. *J. Alloys. Compd.* **2019**, *807*, 151670. DOI

27. Wu, P.; Liu, H.; Xie, Z.; et al. Excellent charge separation of NCQDs/ZnS nanocomposites for the promotion of photocatalytic $H_2$ evolution. *ACS. Appl. Mater. Interfaces.* **2024**, *16*, 16601-11. DOI
28. Khan, M. M.; Abdulwahab, K. O. Metals- and non-metals-doped ZnS for various photocatalytic applications. *Mater. Sci. Semicond. Process.* **2024**, *181*, 108634. DOI
29. Mani, A. D.; Ghosal, P.; Subrahmanyam, C. Novel synthesis of C, N doped rice grain shaped ZnS nanomaterials - towards enhanced visible light photocatalytic activity for aqueous pollutant removal and $H_2$ production. *RSC. Adv.* **2014**, *4*, 23292-8. DOI
30. Peng, H.; Liu, D.; Zheng, X.; Fu, X. N-doped Carbon-coated ZnS with sulfur-vacancy defect for enhanced photocatalytic activity in the visible light region. *Nanomaterials. (Basel).* **2019**, *9*, 1657. DOI PubMed PMC
31. Dharmaraja, C.; Nicholas, P. E.; Ramya, P.; Premkumar, I. I.; Vijayan, V.; Senthilkumar, N. Investigation on photocatalytic activity of ZnS/$NiFe_2O_4$ NCs under sunlight irradiation via a novel two-step synthesis approach. *Inorg. Chem. Commun.* **2021**, *126*, 108481. DOI
32. Jobzari, H.; Iranmanesh, P.; Sabet, M.; Saeednia, S. Effect of synthesis method and chemical reagents on the structural parameters, particle size, and optical and photoluminescence properties of ZnS nanostructures. *Luminescence* **2019**, *34*, 689-98. DOI PubMed
33. Lange, T.; Reichenberger, S.; Ristig, S.; et al. Zinc sulfide for photocatalysis: white angel or black sheep? *Prog. Mater. Sci.* **2022**, *124*, 100865. DOI
34. Stefan, M.; Toloman, D.; Popa, A.; et al. Interface charge transfer process in ZnO:Mn/ZnS nanocomposites. *J. Nanopart. Res.* **2016**, *18*, 3369. DOI
35. Suganthi, N.; Pushpanathan, K. Photocatalytic degradation and antimicrobial activity of transition metal doped mesoporous ZnS nanoparticles. *Int. J. Environ. Sci. Technol.* **2019**, *16*, 3375-88. DOI
36. Wang, W.; Lee, G.; Wang, P.; Qiao, Z.; Liu, N.; Wu, J. J. Microwave synthesis of metal-doped ZnS photocatalysts and applications on degrading 4-chlorophenol using heterogeneous photocatalytic ozonation process. *Sep. Purif. Technol.* **2020**, *237*, 116469. DOI
37. Starukh, H.; Praus, P. Doping of graphitic carbon nitride with non-metal elements and its applications in photocatalysis. *Catalysts* **2020**, *10*, 1119. DOI
38. Talukdar, S.; Dutta, R. K. A mechanistic approach for superoxide radicals and singlet oxygen mediated enhanced photocatalytic dye degradation by selenium doped ZnS nanoparticles. *RSC. Adv.* **2016**, *6*, 928-36. DOI
39. Shao, Y.; Jiang, Z.; Zhang, Q.; Guan, J. Progress in nonmetal-doped graphene electrocatalysts for the oxygen reduction reaction. *ChemSusChem* **2019**, *12*, 2133-46. DOI
40. Li, Z.; Lu, X.; Teng, J.; Zhou, Y.; Zhuang, W. Nonmetal-doping of noble metal-based catalysts for electrocatalysis. *Nanoscale* **2021**, *13*, 11314-24. DOI
41. Wang, Y.; Chen, Y.; Barakat, T.; et al. Recent advances in non-metal doped titania for solar-driven photocatalytic/photoelectrochemical water-splitting. *J. Energy. Chem.* **2022**, *66*, 529-59. DOI
42. Zou, M.; Feng, L.; Ganeshraja, A. S.; Xiong, F.; Yang, M. Defect induced nickel, nitrogen-codoped mesoporous $TiO_2$ microspheres with enhanced visible light photocatalytic activity. *Solid. State. Sci.* **2016**, *60*, 1-10. DOI
43. Wu, Y.; Zhuang, Z.; Chen, C.; Li, J.; Xiao, F.; Chen, C. Atomic-level regulation strategies of single-atom catalysts: nonmetal heteroatom doping and polymetallic active site construction. *Chem. Catal.* **2023**, *3*, 100586. DOI
44. Khan, S.; Je, M.; Ton, N. N. T.; et al. C-doped ZnS-ZnO/Rh nanosheets as multijunctioned photocatalysts for effective $H_2$ generation from pure water under solar simulating light. *Appl. Catal. B. Environ.* **2021**, *297*, 120473. DOI
45. Muruganandham, M.; Kusumoto, Y. Synthesis of N, C Codoped hierarchical porous microsphere ZnS as a visible light-responsive photocatalyst. *J. Phys. Chem. C.* **2009**, *113*, 16144-50. DOI
46. Riazian, M. Enhancement of the photocatalytic activity of fabricated ZnS nanoparticles in the photodegradation of methylene blue. *Phys. Scr.* **2023**, *98*, 065956. DOI
47. Al-Kahtani, A. A.; Alshehri, S. M.; Naushad, M.; Ruksana; Ahamad, T. Fabrication of highly porous N/S doped carbon embedded with ZnS as highly efficient photocatalyst for degradation of bisphenol. *Int. J. Biol. Macromol.* **2019**, *121*, 415-23. DOI PubMed
48. Zhu, B.; Zhou, J.; Ni, L.; Diao, G. Synthesis and characterization of P-doped g-$C_3N_4$ nanosheet hybridized ZnS nanospheres with enhanced visible-light photocatalytic activity. *J. Solid. State. Chem.* **2022**, *305*, 122703. DOI
49. Wan, H.; Xu, L.; Huang, W.; et al. Band engineering of ZnS by codoping for visible-light photocatalysis. *Appl. Phys. A.* **2014**, *116*, 741-50. DOI
50. Bao, L.; Dai, C.; Liu, C.; et al. Fluorine lattice-doped ZnS with accompanying sulfur vacancies for high activity and selectivity of $CO_2$ conversion to CO. *Ceram. Int.* **24**, *50*, 19769-80. DOI
51. Abid, N.; Khan, A. M.; Shujait, S.; et al. Synthesis of nanomaterials using various top-down and bottom-up approaches, influencing factors, advantages, and disadvantages: a review. *Adv. Colloid. Interface. Sci.* **2022**, *300*, 102597. DOI
52. Tairi, L.; Messai, Y.; Bourzami, R.; et al. Enhanced photoluminescence and photocatalytic activity of $Ca^{2+}$ addition into ZnS nanoparticles synthesized by hydrothermal method. *Physica. B:. Condensed. Matter.* **2022**, *631*, 413713. DOI
53. Samanta, D.; Basnet, P.; Jha, S.; Chatterjee, S. Proficient route in synthesis of glucose stabilized Ag modified ZnS nanospheres for mechanistic understandings of commercially used dyes degradation. *Inorg. Chem. Commun.* **2022**, *141*, 109498. DOI
54. Poornaprakash, B.; Chalapathi, U.; Kumar, M.; et al. Tailoring the optical, magnetic, and photocatalytic properties of ZnS quantum dots by rare-earth ion doping. *Chemical. Physics. Letters.* **2020**, *753*, 137609. DOI
55. Poornaprakash, B.; Chalapathi, U.; Suh, Y.; Vattikuti, S. P.; Reddy, M. S. P.; Park, S. Terbium-doped ZnS quantum dots: structural, morphological, optical, photoluminescence, and photocatalytic properties. *Ceramics. International.* **2018**, *44*, 11724-9. DOI

56. Li, S. Hydrothermal synthesis of Cu-doped ZnS for enhanced photocatalytic degradation of tetracycline under the visible light. *IOP. Conf. Ser:. Earth. Environ. Sci.* **2021**, *769*, 022053. DOI
57. Dake, D. V.; Raskar, N. D.; Mane, V. A.; et al. Exploring the role of defects on diverse properties of Cr-substituted ZnS nanostructures for photocatalytic applications. *Appl. Phys. A.* **2020**, *126*, 3669. DOI
58. Dake, D. V.; Raskar, N. D.; Mane, V. A.; et al. Intriguing physicochemical properties and impact of co-dopants on N-doped graphene oxide based ZnS nanowires for photocatalytic application. *Sci. Rep.* **2023**, *13*, 7595. DOI PubMed PMC
59. Zhao, W.; Wei, Z.; Wu, X.; Zhang, X.; Zhang, L.; Wang, X. Microstructure and photocatalytic activity of Ni-doped ZnS nanorods prepared by hydrothermal method. *Trans. Nonferrous. Met. Soc. China.* **2019**, *29*, 157-64. DOI
60. Wang, R.; Liang, H.; Hong, J.; Wang, Z. Hydrothermal synthesis of cobalt-doped ZnS for efficient photodegradation of methylene blue. *J. Photoch. Photobio. A.* **2016**, *325*, 62-7. DOI
61. Bui, H. V.; Thai, D. V.; Nguyen, T. D.; et al. Mn-doped ZnS nanoparticle photoanodes: synthesis, structural, optical, and photoelectrochemical characteristics. *Mater. Chem. Phys.* **2023**, *307*, 128081. DOI
62. Govindasamy, K.; Senthilkumar, S. Green synthesis of Mn-doped ZnO nanoparticles using ipomoea staphylina leaf extract: characterization and application of photocatalytic dye degradation, antibacterial and antioxidant activity. *Chemistryselect* **2024**, *9*, e202402347. DOI
63. Sharma, J.; Gupta, A.; Pandey, O. Effect of Zr doping and aging on optical and photocatalytic properties of ZnS nanopowder. *Ceram. Int.* **2019**, *45*, 13671-8. DOI
64. Sonkar, R.; Mondal, N. J.; Thakur, S.; Saikia, E.; Ghosh, M. P.; Chowdhury, D. Cobalt-substituted ZnS QDs: a diluted magnetic semiconductor and efficient photocatalyst. *Nanoscale. Adv.* **2023**, *5*, 7042-56. DOI PubMed PMC
65. Suganthi, N.; Pushpanathan, K. Photocatalytic degradation and ferromagnetism in mesoporous La doped ZnS nanoparticles. *J. Mater. Sci:. Mater. Electron.* **2018**, *29*, 13970-83. DOI
66. Yaemphutchong, S.; Wattanathana, W.; Deeloed, W.; et al. Characterization, luminescence and dye adsorption study of manganese and samarium doped and co-doped zinc sulfide phosphors. *Opt. Mater.* **2020**, *107*, 109965. DOI
67. Amani-Ghadim, A. R.; Arefi-Oskoui, S.; Mahmoudi, R.; et al. Improving photocatalytic activity of the ZnS QDs via lanthanide doping and photosensitizing with GO and g-$C_3N_4$ for degradation of an azo dye and bisphenol-A under visible light irradiation. *Chemosphere* **2022**, *295*, 133917. DOI
68. Khaparde, R.; Acharya, S. Effect of isovalent dopants on photodegradation ability of ZnS nanoparticles. *Spectrochim. Acta. A. Mol. Biomol. Spectrosc.* **2016**, *163*, 49-57. DOI PubMed
69. Labiadh, H.; Chaabane, T. B.; Balan, L.; et al. Preparation of Cu-doped ZnS QDs/$TiO_2$ nanocomposites with high photocatalytic activity. *Appl. Catal. B:. Environ.* **2014**, *144*, 29-35. DOI
70. Latief, U.; Islam, S. U.; Khan, Z.; Shahid, K. M. Luminescent Manganese/Europium doped ZnS quantum dots: Tunable emission and their application as fluorescent sensor. *J. Alloys. and. Compd.* **2022**, *910*, 164889. DOI
71. Madkour, M.; Ali, A. A.; Sagheer, F. A.; Nazeer, A. A. Solar active $Cu^{2+}$-ZnS photocatalyst for efficient photodegradation of 4-chlorophenol: effective cation doping effect. *Catal. Today.* **2021**, *379*, 7-14. DOI
72. Ramki, K.; Rajapriya, A.; Sakthivel, P.; Murugadoss, G.; Thangamuthu, R.; Rajesh, K. M. Rapid degradation of organic dyes under sunlight using tin-doped ZnS nanoparticles. *J. Mater. Sci:. Mater. Electron.* **2020**, *31*, 8750-60. DOI
73. Sharath, D.; Gaikwad, A.; Choudhury, S.; Gupta, N.; Sasikala, R.; Betty, C. Effect of Indium doping on the photoelectrochemical and photocatalytic properties of zinc sulphide. *Mater. Sci. Eng:. B.* **2017**, *226*, 57-63. DOI
74. Shah, U.; Jan, F. A.; Ullah, R.; Wajidullah; Salman; Ullah, N. Tin decorated zinc sulphide nanoparticles for photocatalytic degradation of bromophenol blue dye and their therapeutic applications: a kinetic and thermodynamic approach. *ECS. J. Solid. State. Sci. Technol.* **2022**, *11*, 033011. DOI
75. Kannan, S.; Subiramaniyam, N.; Sathishkumar, M. Effect of annealing temperature and Mn doping on the structural and optical properties of ZnS thin films for enhanced photocatalytic degradation under visible light irradiation. *Inorg. Chem. Commun.* **2020**, *119*, 108068. DOI
76. Khan, J. A.; Ahamad, S.; Ansari, M. A. H.; et al. State-of-the-art in ZnS-based nanoarchitects for visible-light photocatalytic degradation of antibiotics and organic dyes. *J. Water. Process. Eng.* **2024**, *67*, 106151. DOI
77. Zhou, Y.; Chen, G.; Yu, Y.; et al. An efficient method to enhance the stability of sulphide semiconductor photocatalysts: a case study of N-doped ZnS. *Phys. Chem. Chem. Phys.* **2015**, *17*, 1870-6. DOI
78. Moon, H.; Goh, M. S.; Cha, M.; et al. Explosive hydrogen evolution from water splitting without sacrificial agent from the C, N co-doped Zn defective ZnS particle. *Appl. Surf. Sci.* **2022**, *606*, 154787. DOI
79. Moon, H.; Kim, S.; Joo, S. W.; et al. Design and selective photocatalytic activity of highly concentrated C, N, O co-doped Zn, S co-defective ZnS particles mediated by ethylenediamine derivatives. *Nano. Today.* **2023**, *49*, 101785. DOI
80. Kouser, S.; Lingampalli, S. R.; Chithaiah, P.; et al. Extraordinary changes in the electronic structure and properties of CdS and ZnS by anionic substitution: cosubstitution of P and Cl in place of S. *Angew. Chem. Int. Ed. Engl.* **2015**, *54*, 8149-53. DOI
81. Wang, C.; You, C.; Rong, K.; Shen, C.; Yang, F.; Li, S. An S-Scheme MIL-101(Fe)-on-BiOCl heterostructure with oxygen vacancies for boosting photocatalytic removal of Cr(VI). *Acta. Physico-Chimica. Sinica.* **2024**, *40*, 2307045. DOI
82. Dong, K.; Shen, C.; Yan, R.; Liu, Y.; Zhuang, C.; Li, S. Integration of plasmonic effect and S-scheme heterojunction into $Ag/Ag_3PO_4/C_3N_5$ photocatalyst for boosted photocatalytic levofloxacin degradation. *Acta. Physico-Chimica. Sinica.* **2024**, *40*, 2310013. DOI

83. Li, S.; Rong, K.; Wang, X.; Shen, C.; Yang, F.; Zhang, Q. Design of carbon quantum dots/CdS/$Ta_3N_5$ S-scheme heterojunction nanofibers for efficient photocatalytic antibiotic removal. *Acta. Physico-Chimica. Sinica.* **2024**, *40*, 2403005. DOI
84. Kanakaraju, D.; Chandrasekaran, A. Recent advances in $TiO_2$/ZnS-based binary and ternary photocatalysts for the degradation of organic pollutants. *Sci. Total. Environ.* **2023**, *868*, 161525. DOI PubMed
85. Krishna, A. M. S.; Ramasubramanian, B.; Haseena, S.; et al. Functionalized graphene-incorporated cupric oxide charge-transport layer for enhanced photoelectrochemical performance and hydrogen evolution. *Catalysts* **2023**, *13*, 785. DOI
86. Li, C.; Zhang, J.; Chen, X.; Tao, H.; Zhou, Y.; Zhu, M. Upgraded charge transfer by an internal electric field in 2D/2D BiOCl/N-rich $C_3N_5$ heterojunctions for efficiently visible-light catalytic NO removal. *Chem. Eng. J.* **2023**, *468*, 143753. DOI
87. Li, S.; You, C.; Xue, Q.; et al. Carbon quantum dots and interfacial chemical bond synergistically modulated S-scheme $Mn_{0.5}Cd_{0.5}S$/BiOBr photocatalyst for efficient water purification. *J. Mater. Sci. Technol.* **2025**, *214*, 255-65. DOI
88. Zhang, J.; Yu, G.; Yang, C.; Li, S. Recent progress on S-scheme heterojunction strategy enabling polymer carbon nitrides $C_3N_4$ and $C_3N_5$ enhanced photocatalysis in energy conversion and environmental remediation. *Curr. Opin. Chem. Eng.* **2024**, *45*, 101040. DOI
89. Tom, E.; Velluva, A.; Joseph, A.; et al. Tailoring the electrochemical properties of ZnS electrodes via cobalt doping for improved supercapacitor application. *J. Electron. Mater.* **2025**, *54*, 451-61. DOI
90. Bailón-ruiz, S. J.; Cedeño-mattei, Y.; Núñez-colón, A. M.; Torres-torres, K. Fast One-step microwave-assisted synthesis of iron-doped ZnS for photocatalytic applications. *Crystals* **2024**, *14*, 699. DOI
91. Hussain, I.; Mohapatra, D.; Dhakal, G.; et al. Different controlled nanostructures of Mn-doped ZnS for high-performance supercapacitor applications. *J. Energy. Storage.* **2020**, *32*, 101767. DOI
92. Grandhi, G. K.; Krishna, M.; Mondal, P.; Viswanatha, R. Cation co-doping into ZnS quantum dots: towards visible light sensing applications. *Bull. Mater. Sci.* **2020**, *43*, 2233. DOI